Energy, Mines and Resources Canada

Énergie, Mines et Ressources Canada

CANMET

Canada Centre for Mineral and Energy Technology

Centre canadien de la technologie des minéraux et de l'énergie

Mining Research Laboratories

Laboratoires de recherche minière

Canada

HIGH TEMPERATURE UNIAXIAL AND TRIAXIAL COMPRESSION TESTS ON URL ROCK SAMPLES FROM BOREHOLES 209-018-EXT4 AND 209-030-DIL1

J.S.O. Lau and B. Gorski November 1990

Mining Research Laboratories
Divisional Report MRL 90-109(TR)

This document is the property of the Canada Centre for Mineral and Energy Technology (CANMET)

Ce document est la propriété du Centre canadien de la technologie des minéraux et de l'énergie (CANMET)

69 pp

MICROMEDIA

91-01594/

HIGH TEMPERATURE UNIAXIAL AND TRIAXIAL COMPRESSION TESTS ON URL ROCK SAMPLES FROM BOREHOLES 209-018-EXT4 AND 209-030-DIL1

by

J.S.O. Lau[1] and B. Gorski[2]

ABSTRACT

A series of ambient room and high temperature uniaxial and triaxial compression tests were conducted on grey granitic core samples obtained from boreholes 209-018-EXT4 and 209-030-DIL1 located at the 240 level of AECL Research's Underground Research Laboratory (URL). Twelve sets of tests were carried out at three temperatures (21° – 25°, 75° and 125° C) and four confining pressures (0, 3.5, 17 and 35 MPa) to study the thermo-mechanical properties of the grey granite.

The failure deviator stress and axial strain at failure were found to increase with increasing confining pressure. Temperatures up to 125° C appeared to have little effect on the failure deviator stress and axial strain, except under the unconfined condition where small reductions were observed.

The tangent Young's modulus and pseudo Young's modulus increased with increasing confining pressure at stress levels below approximately 60% of the failure deviator stress. Heating up to 125° C had very little effect on these two moduli, except under the unconfined condition and at the confining pressure of 17 MPa where small reductions in the modulus values were observed.

The strength properties of the rock were expressed in terms of the Hoek and Brown failure criterion. When the temperature was raised from 25° to 75° and then to

---

[1]Geotechnical Engineer, AECL Research, on attachment to Canadian Mine Technology Laboratory, Mining Research Laboratories, CANMET, Energy, Mines and Resources Canada, Ottawa, Ontario.

[2]Rock Mechanics and Development Technologist, Canadian Mine Technology Laboratory, Mining Research Laboratories, CANMET, Energy, Mines and Resources Canada, Ottawa, Ontario.

125° C, the predicted uniaxial compressive strength of the intact rock material, σ_c, was found to increase and then decrease; and the material constant, m, was found to decrease and then increase to approximately their original values. The Hoek and Brown failure envelopes derived from these tests show small reductions in strength at 75° C.

The Mohr-Coulomb friction angle, ϕ, decreased and the cohesive strength, c, increased with increasing confining pressure. Temperatures up to 125° C appeared to have no effect on ϕ and c.

Keywords: uniaxial, triaxial, compression, temperature, confining pressure, strength, strain, modulus, Hoek-Brown, Mohr-Coulomb

ESSAIS DE COMPRESSION UNIAXIALE ET TRIAXIALE À HAUTE TEMPÉRATURE SUR DES ÉCHANTILLONS DE ROCHE DES SONDAGES 209-018-EXT4 ET 209-030-DIL1 DU LRS

par

J.S.O. Lau[1] et B. Gorski[2]

RÉSUMÉ

Une série d'essais de compression uniaxiale et triaxiale à température normale et à température élevée ont été menés sur des échantillons de carotte granitique grise provenant des sondages 209-018-EXT4 et 209-030-DIL1 situés au niveau 240 du Laboratoire de recherche souterrain (LRS) de EACL Recherche. Douze séries d'essais ont été menés à trois températures (21° – 25°, 75° et 125° C) et à quatre pressions de confinement (0, 3.5, 17 et 35 MPa) pour étudier les propriétés thermo-mécaniques du granite gris.

Les essais ont montré que la contrainte de déviation de rupture et la déformation axiale de rupture augmentent avec la pression de confinement. Les températures supérieures à 125° C n'ont pas semblé influé beaucoup sur la contrainte de déviation de rupture et la déformation axiale, sauf en l'absence de confinement où de faibles réductions ont été observées.

Le module tangent de Young et le pseudo-module de Young ont augmenté avec la pression de confinement à des niveaux de contraintes inférieurs à 60% environ de la contrainte de rupture. Portée à 125° C, la température a très peu influé sur ces deux modules, sauf en l'absence de confinement et à la pression de confinement de 17 MPa où de faibles réductions des modules ont été observées.

Les propriétés de résistance de la roche ont été exprimées en termes du critère de rupture de Hoek et Brown. Lorsque la température a été portée de 25° à 75°, puis à 125° C, la résistance prévue à la compression uniaxiale dans la

---

[1]Ingénieur en géotechnique, EACL Recherche, affecté au Laboratoire canadien de technologie minière, Laboratories de recherche minière, CANMET, Énergie, Mines et Ressources Canada, Ottawa, Ontario.

[2]Technologue en mécanique des roches et développement, Laboratoire canadien de technologie minière, Laboratoires de recherche minière, CANMET, Énergie, Mines et Ressources Canada, Ottawa, Ontario.

roche intacte, σ_c, a augmenté, puis diminué, et la constante de matériau, m, a diminué, puis augmenté pour revenir à leur valeur initiale. Les enveloppes de rupture de Hoek et Brown, établies par ces essais, présentent de faibles réductions de résistance à 75° C.

L'angle de frottement de Mohr-Coulomb, ϕ, a diminué, et la résistance de cohésion, c, a augmenté en fonction de la pression de confinement. Des températures allant jusqu'à 125° C ont semblé n'avoir aucun effet sur ϕ et c.

Mots clés: uniaxiale, triaxiale, compression, température, pression de confinement, résistance, déformation, module, Hoek-Brown, Mohr-Coulomb

CONTENTS

	Page
ABSTRACT	i
RÉSUMÉ	iii
INTRODUCTION	1
SAMPLING AND SPECIMEN PREPARATION	2
DYNAMIC ELASTIC PROPERTIES	2
TEST APPARATUS AND PROCEDURE	3
TESTING PROGRAM	4
RESULTS AND DISCUSSION	4
Test Results	4
Failure Deviator Stress	5
Axial Strain at Failure	6
Tangent Young's Modulus	6
Pseudo Young's Modulus	7
Poisson's Ratio	7
Strength Properties	8
CONCLUSIONS	11
RECOMMENDATIONS	12
ACKNOWLEDGEMENTS	13
REFERENCES	13
APPENDIX A	34

TABLES

No.		
1.	Dimensions, densities and dynamic elastic properties of rock specimens.	15
2.	Results of ambient room and high temperature uniaxial and triaxial compression tests.	16
3.	Tangent Young's moduli at stress levels ranging from 10 to 90% of the failure deviator stress.	18
4.	Pseudo Young's moduli at stress levels ranging from 10 to 90% of the failure deviator stress.	20

5. Mean values and standard deviations (in brackets) of failure deviator stress, axial strains at failure, tangent Young's modulus and pseudo Young's modulus. 22
6. Values of σ_c, m, s, r^2, σ_{cmass} and σ_{tmass} derived from the Hoek and Brown failure criterion. 23
7. Values of the Mohr-Coulomb friction angle ϕ and cohesive strength c. 24

FIGURES

1. Plots of failure deviator stress versus temperature. 25
2. Plots of axial strain at failure versus temperature. 26
3. Plots of mean tangent Young's modulus at the stress level of 50% of $(\sigma_1 - \sigma_3)_f$ versus temperature. 27
4. Plots of mean pseudo Young's modulus at the stress level of 50% of $(\sigma_1 - \sigma_3)_f$ versus temperature. 28
5. Plots of Poisson's ratio versus temperature. 29
6. Hoek and Brown failure envelope for tests conducted at 21° – 25° C. 30
7. Hoek and Brown failure envelope for tests conducted at 75° C. 31
8. Hoek and Brown failure envelope for tests conducted at 125° C. 32
9. Effect of temperature on the Hoek and Brown failure envelope. 33

INTRODUCTION

As part of the Canadian Nuclear Fuel Waste Management Program (CNFWMP) concerned with the long-term disposal of high level nuclear wastes in vaults located at depth in plutonic rocks, AECL Research has constructed the Underground Research Laboratory (URL) located near to Lac du Bonnet, Manitoba to provide a representative environment in which large-scale geotechnical and hydrogeological investigations can be conducted. In support of the geomechanical investigations at the URL, a joint laboratory testing and analysis program on URL core samples has been undertaken by the Canada Centre for Mineral and Energy Technology (CANMET) and AECL Research to provide data on the mechanical properties of the rock mass surrounding the URL excavation, under both ambient room and high temperature conditions. This information is necessary for the development of the geotechnical data base for the URL characterization program, and is also required by numerical modellers for input into geomechanical models and by engineers for the design of the experiments to be carried out at the URL.

Two series of uniaxial and triaxial compression tests at ambient room and high temperatures were conducted in CANMET in 1988 and 1989 on core samples of grey granite from boreholes 209-021-SV1 and 209-030-DIL1 located in Room 209 at the 240 level of the URL and the results were presented in CANMET divisional reports MRL 88-112(TR) (Lau et al., 1988) and MRL 89-90(TR) (Lau and Gorski, 1989). It was noted that the effect of heating to 125° C on the mechanical properties of the grey granite can be masked by intrinsic differences in samples obtained from boreholes with different orientations. Rock samples from borehole 209-021-SV1 (trend = 046.38°, plunge = −04.89°), drilled at the northeast side of Room 209, were found to be consistently stronger and stiffer than those from borehole 209-030-DIL1 (trend = 209.92°, plunge = −02.83°), drilled at the southwest side of Room 209. It has been concluded that a meaningful study on the effect of heating on the mechanical properties of the rock can be carried out only if samples from a cluster of boreholes with similar orientations are used in the same study.

One study, using core samples from two boreholes, drilled in the northeast/subhorizontal (trend/plunge) direction at the northeast side of Room 209, was completed earlier this year and the results have been reported by Lau and Gorski (1990). Another study, using core samples from two boreholes, 209-030-DIL1 and 209-018-EXT4 (trend = 211.05°, plunge = −01.03°), drilled in the southwest/subhorizontal direction at the southwest side of Room 209, was completed in the fall of 1990, and the results are presented and discussed in this report.

SAMPLING AND SPECIMEN PREPARATION

Samples used in these tests were NQ rock cores from boreholes 209-018-EXT4 and 209-030-DIL1. The rock is a grey, medium- to coarse-grained granite, composed of approximately 30% K-feldspar, 30% plagioclase, 30% or slightly less quartz and 10% or slightly more mafic minerals, mainly biotite.

Specimens were prepared in accordance with the procedure described in the Pit Slope Manual Supplement 3-5 (Gyenge and Ladanyi, 1977) and the method suggested by the International Society for Rock Mechanics (Brown, 1981). The end surfaces of each of the specimens were ground flat to 0.025 mm to ensure that the end surfaces were parallel to each other and perpendicular to the axis of the specimen. The lengths, diameters and bulk densities of the specimens are shown in Table 1. It should be noted that in Table 1, the last number in the specimen identification represents the downhole length of the specimen. The mean bulk density of all the specimens was found to be 2.64 Mg/m^3. The specimen lengths varied from 98.58 to 116.10 mm and the diameters varied from 44.84 to 45.06 mm, with length to diameter ratios ranging from 2.2 to 2.6.

DYNAMIC ELASTIC PROPERTIES

Prior to the uniaxial and triaxial testing, compression (p) and shear (s) wave velocity measurements were made on the rock specimens. The purpose of the p- and s-wave measurements is to estimate various mechanical rock properties non-destructively prior to actual testing. The velocity measurements were made in accordance with the procedure described in the Pit Slope Manual Supplement 3-2 (Gyenge and Herget, 1977), using a pulse generator, pulsing and sensing heads and a Tektronix 2230 digital storage oscilloscope. The p- and s-wave velocities were determined from their respective transit times along the longitudinal axes of the specimens. The dynamic elastic constants were computed from the measured wave velocities and the bulk density, using the following equations:

Dynamic Young' modulus of elasticity:

$$E_u = \frac{\rho V_s^2 (3V_p^2 - 4V_s^2)}{V_p^2 - V_s^2} \qquad (1)$$

where E_u = dynamic Young's modulus of elasticity
V_p = compression wave velocity
V_s = shear wave velocity
ρ = bulk density

Dynamic shear modulus:

$$G_u = \rho V_s^2 \tag{2}$$

where G_u = dynamic shear modulus

Dynamic Poisson's ratio:

$$\nu_u = \frac{V_p^2 - 2V_s^2}{2(V_p^2 - V_s^2)} \tag{3}$$

where ν_u = dynamic Poisson's ratio

The p-wave velocity, s-wave velocity, dynamic Young's modulus, dynamic shear modulus and dynamic Poisson's ratio determined for each of the specimens are given in Table 1. Table 1 also shows the mean values and standard deviations of the wave velocities and the dynamic elastic constants. The samples were found to have mean values of 4.315 km/s for p-wave velocity, 2.561 km/s for s-wave velocity, 42.49 GPa for dynamic Young's modulus, 17.33 GPa for dynamic shear modulus and 0.23 for dynamic Poisson's ratio. These values are considerably lower than those determined for core samples from boreholes 209-021-SV1 and 209-025-SV2 (Lau and Gorski, 1990), suggesting that more microcracks were present in the samples used for this study.

TEST APPARATUS AND PROCEDURE

The uniaxial and triaxial compression tests were conducted using a computer-controlled, servo-hydraulic test system, the MTS 815 Rock Mechanics Test System, consisting of a 2.22 MN rated load cell, load frame, hydraulic power supply, triaxial cell, test controller, test processor, temperature controller and DEC micro PDP 11/73 computer. The triaxial cell is rated up to 200° C and equipped with a heater, heat shroud, thermocouples, three linear variable differential transducers (LVDTs) for the measurement of axial strain and an extensometer with a circumferential kit for the measurement of circumferential strain. For a detailed description of the MTS system and its operation, the reader is referred to the MTS Operation Manual (MTS Systems Corp., 1986) and CANMET Division Report MRL 87-33(INT) (Gorski, 1987).

In the high temperature triaxial tests, specimens encapsulated in Teflon shrink tubing were heated to the test temperature under confinement prior to the testing. The uniaxial and triaxial test procedures have been described in CANMET divisional reports MRL 89-90(TR) (Lau and Gorski, 1989) and MRL 88-112(TR) (Lau et al., 1988) respectively, and therefore will not be repeated here.

TESTING PROGRAM

Testing for this study took place between October, 1988 and October, 1990 at Canadian Mine Technology Laboratory, Mining Research Laboratories, CANMET, Energy, Mines and Resources Canada in Ottawa. The testing program consisted of twelve sets of tests conducted under the unconfined condition and at the confining pressures of 3.5, 17 and 35 MPa and at the test temperatures of 21° – 25°, 75° and 125° C. The testing program is summarized in Table 2. A minimum of three tests were carried out in each set under the same confining pressure and temperature conditions in order to obtain statistically meaningful mean values. A total of 41 tests were performed for this study.

RESULTS AND DISCUSSION

TEST RESULTS

Table 2 summarizes the axial strain at failure, failure deviator stress, tangent Young's modulus and pseudo Young's modulus at a stress level equivalent to 50% of the failure deviator stress, Poisson's ratio, failure angle, θ, and failure characteristics of each of the specimens. It should be noted that results from four tests were rejected due to their incompatibility with the rest. The measurement of the axial strain was made using three LVDTs while the circumferential strain was measured using the bicycle chain extensometer. Each axial strain, presented in Table 2 and illustrated in the stress-strain curve in Appendix A, is the average of the axial deformations obtained from the three LVDTs divided by the specimen length. The Poisson's ratio was determined as the ratio of the axial to the circumferential tangent moduli at the stress level equivalent to 50% of the failure deviator stress. The effects of the confining pressure and temperature on the strength and deformability of the rock samples will be discussed in the following subsections.

Stress versus strain curves for tests conducted in 1990 are presented in Appendix A of this report. Stress-strain curves for tests performed in 1988 and 1989 have been presented in CANMET divisional reports MRL 88-112(TR) and MRL 89-90(TR) and therefore will not be repeated in this report. These curves were plotted by the use of DATAPLOT curve fitting computer software. A cubic spline fit was used for this analysis which employed a third degree equation model of the form:

$$\sigma = a_0 + a_1\varepsilon + a_2\varepsilon^2 + a_3\varepsilon^3 \qquad (4)$$

where σ = stress

ε = strain

and a_0, a_1, a_2 and a_3 are coefficients

FAILURE DEVIATOR STRESS

One of the main objectives of these tests is to study the effects of confining pressure and temperature on the strength of the rock specimens. The failure deviator stresses of the specimens and their mean values at different confining pressure and temperature conditions are shown in Tables 2 and 5 respectively. Note that in Table 5, the standard deviations are given in brackets. The failure deviator stresses and their mean values are also plotted against temperature in Figure 1. It can be seen that the failure deviator stress increased as the confining pressure increased.

Temperature appeared to have little effect on the failure deviator stress. Under the unconfined condition, the mean failure deviator stress decreased by only 2.3% as the temperature was raised from 25° to 125° C. At the confining pressure of 3.5 MPa, the mean failure deviator stress increased by 1.6% as the temperature was increased to 75° C. However, when the temperature was further increased to 125° C, a net reduction of 0.6% was resulted. At the confining pressure of 17 MPa, virtually no change in the failure deviator stress was observed as the temperature was raised to 125° C. At the highest confining pressure of 35 MPa, the mean failure deviator stress decreased by 3.3% as the temperature was increased from 21° to 75° C. When the temperature was raised from 75° to 125° C, the mean failure deviator increased because higher failure deviator stresses were recorded in two tests conducted at 125° C. As a result, the net reduction in the mean failure deviator stress at 125° C was only 1.3%.

AXIAL STRAIN AT FAILURE

The axial strains at failure and their mean values at the four confining pressures and three test temperatures are given in Tables 2 and 5 respectively, and are also plotted versus temperature in Figure 2. They show that the axial strain at failure increased as the confining pressure increased. Temperature did not have much effect on the axial strain at failure, except under the unconfined condition where an 8.5% decrease was observed when the temperature was raised to 75° C. However, no change in the mean axial strain was observed when the temperature was further increased to 125° C. Under the confined conditions, the axial strain at failure in general decreased slightly when the temperature was raised to 125° C. The mean axial strains at the confining pressures of 3.5 and 35 MPa were observed to increase slightly when the temperature was raised from 75° to 125° C. The reason for this behaviour is that, in both cases, very high axial strain was recorded in one of the tests conducted at 125° C. Nevertheless, net reductions of 1.7, 2.9 and 1.9% were recorded at the confining pressures of 3.5, 17 and 35 MPa respectively when the temperature was raised from 25° to 125° C.

TANGENT YOUNG'S MODULUS

Tangent Young's moduli for each of the rock specimens were computed from the stress-strain curve at nine stress levels equal to 10, 20, 30, 40, 50, 60, 70, 80 and 90% of the failure deviator stress, $(\sigma_1 - \sigma_3)_f$, and are presented in Table 3. The tangent moduli were determined by substituting the axial strain values corresponding to those nine stress levels into the derivatives of the best-fit equations (Equation 4) representing the stress-strain curve.

The tangent Young's modulus varied at different stress levels. Under the unconfined condition, the tangent modulus increased until approximately 60% of $(\sigma_1 - \sigma_3)_f$ was reached and then decreased until failure. At higher confining pressures, the tangent modulus behaved similarly, reaching the maximum values at approximately 50% and 20% of $(\sigma_1 - \sigma_3)_f$ at the confining pressures of 3.5 and 17 MPa respectively. At the highest confining pressure of 35 MPa, the tangent modulus decreased slowly with increasing deviator stress.

The effect of confining pressure on the tangent modulus is considerable at stress levels below approximately 50% of $(\sigma_1 - \sigma_3)_f$. The tangent modulus at those stress levels increased as the confining pressure increased, especially at the onset of loading (low stress levels), suggesting that some stress relaxation had occurred in these specimens, resulting in larger deformations and lower modulus values at low confining pressures

and low stress levels. At 50% of $(\sigma_1 - \sigma_3)_f$, the modulus increased only when the confining pressure increased from 0 to 3.5 MPa (Fig. 3). At the stress levels above 60% of $(\sigma_1 - \sigma_3)_f$, the confining pressure appeared to have no effect on the tangent modulus.

The mean 50% (at the stress level of 50% of $(\sigma_1 - \sigma_3)_f$) tangent Young's moduli at different confining pressures and test temperatures are shown in Table 5. The mean 50% tangent moduli were also plotted against temperature in Figure 3. The modulus-temperature plots show that temperatures up to 125° C had little effect on the tangent modulus at the confining pressures of 3.5 and 35 MPa. Under the unconfined condition and at the confining pressure of 17 MPa, reductions of only 2.5 and 2.9% respectively were observed at the temperature of 125° C.

PSEUDO YOUNG'S MODULUS

Actual stress versus axial strain curves for these specimens are nonlinear (see Appendix A). For modelling purposes, each nonlinear curve may be idealized as a series of straight lines joining points corresponding to stress levels of 0.0, 0.1, 0.2, 0.3, 0.4, 0.5, 0.6, 0.7, 0.8, 0.9 and 1.0 times the failure deviator stress. The slope of each of those straight lines is defined as the pseudo Young's modulus. The pseudo Young's moduli of the rock specimens are presented in Table 4. In general, the pseudo moduli are lower than the tangent moduli at low stress levels, especially at low confining pressures, but higher than the tangent moduli at high stress levels.

The effects of confining pressure and temperature on the pseudo Young's modulus are similar to those on the tangent modulus. The pseudo modulus increased with increasing confining pressure only at stress levels below approximately 60% of $(\sigma_1 - \sigma_3)_f$. The mean 50% pseudo Young's moduli are shown in Table 5 and plotted against temperature in Figure 4. The plots show that temperatures up to 125° C also had little effect on the pseudo modulus. Only 2.9 and 3.3% reductions in the mean modulus values were observed under the unconfined condition and at the confining pressure of 17 MPa respectively.

POISSON'S RATIO

The Poisson's ratios obtained from these tests are presented in Table 2. It should be noted that there are uncertainties in the determination of the values of Poisson's ratio. The value depends strongly on the method of calculation. For this report, the Poisson's ratio was determined from the ratio of the axial to the circumferential tangent moduli

at the stress level equivalent to 50% of the failure deviator stress. Values determined at other stress levels will be different from the values presented in this report.

The Poisson's ratios and their mean values (Table 5) are plotted versus temperature in Figure 5. The plots show that the mean Poisson's ratio increased with increasing confining pressure up to the confining pressure of 17 MPa. No significant change in the mean values was observed when the confining pressure was increased from 17 to 35 MPa.

Heating up to 125° C reduced the mean Poisson's ratio by 9.1, 16.0 and 10.8% under the unconfined condition and at the confining pressures of 17 and 35 MPa respectively. At the confining pressure of 3.5 MPa, the mean Poisson's ratio increased slightly by 1.8% when the temperature was raised to 125° C. The discrepancy is probably due to the uncertainties in the determination of the values of Poisson's ratio.

STRENGTH PROPERTIES

The strength properties of the intact rock specimens can be expressed in terms of the Hoek and Brown failure criterion. The empirical relationship developed by Hoek and Brown (1980) between the principal stresses associated with the failure of a rock is given as follows:

$$\sigma_1 = \sigma_3 + \sqrt{m\sigma_c\sigma_3 + s{\sigma_c}^2} \tag{5}$$

where σ_1 = major principal stress at failure
σ_3 = minor principal stress applied to the rock sample
σ_c = uniaxial compressive strength of the intact rock material in the specimen
m and s are constants

According to the criterion, the values of m and s depend on the properties of the rock and the extent to which the rock has been broken before being subjected to the principal stresses σ_1 and σ_3. For these intact rock specimens, $s = 1$, and the uniaxial compressive strength of the intact rock material, σ_c, and the material constant, m, can be computed by using the following equations:

$$\sigma_c^2 = \frac{\sum y_i}{n} - \left[\frac{\sum x_i y_i - \frac{\sum x_i \sum y_i}{n}}{\sum x_i^2 - \frac{(\sum x_i)^2}{n}}\right]\frac{\sum x_i}{n} \tag{6}$$

$$m = \frac{1}{\sigma_c}\left[\frac{\sum x_i y_i - \frac{\sum x_i \sum y_i}{n}}{\sum x_i^2 - \frac{(\sum x_i)^2}{n}}\right] \tag{7}$$

where $x = \sigma_3$

$y = (\sigma_1 - \sigma_3)^2$

n = total number of data pairs x_i and y_i

The coefficient of determination r^2 is given by:

$$r^2 = \frac{\left[\sum x_i y_i - \frac{\sum x_i \sum y_i}{n}\right]^2}{\left[\sum x_i^2 - \frac{(\sum x_i)^2}{n}\right]\left[\sum y_i^2 - \frac{(\sum y_i)^2}{n}\right]} \tag{8}$$

The closer the value of r^2 is to 1.00, the better the fit between Equation 5 and the test data is.

Hoek and Brown failure envelopes for tests conducted at the temperatures of $21° - 25°$, 75° and 125° C were generated, using Equation 5, and are shown in Figures 6, 7 and 8 respectively. The values of σ_c, m and r^2, computed by using Equations 6, 7 and 8, are presented in Table 6. The coefficient of determination, r^2, was found to range from 0.9827 to 0.9983, indicating that the fit of Equation 5 to the data was good. The predicted uniaxial compressive strength of the intact rock material, σ_c, was found to increase from 171 to 180 MPa when the temperature was raised from room temperature to 75° C, and then decrease to 172 MPa when the temperature was further increased to 125° C. The m value was found to decrease from 36.32 to 32.09 as the temperature was raised to 75° C, and then increase to 35.39 as the temperature was raised to 125° C. In Figure 9, all three failure envelopes are plotted. They show a slight decrease in the strength of the rock at the temperature of 75° C and almost no change at the temperature of 125° C.

Hoek (1990) suggests that the uniaxial compressive strength of the rock mass, σ_{cmass}, can be computed by substituting $\sigma_3 = 0$ into Equation 5, yielding:

$$\sigma_{cmass} = \sqrt{s}\sigma_c \tag{9}$$

and the uniaxial tensile strength of the rock mass, σ_{tmass}, can be calculated by substituting $\sigma_1 = 0$ into Equation 5 and solving the resulting quadratic equation:

$$\sigma_{tmass} = \frac{\sigma_c}{2}(m - \sqrt{m^2 + 4s}) \tag{10}$$

The values of σ_{cmass} and σ_{tmass} derived from these tests, assuming $s = 1$, are also given in Table 6. It can be seen that temperature had little effect on σ_{cmass} and σ_{tmass}. Both σ_{cmass} and σ_{tmass} increased as the temperature was raised from room temperature to 75° C, and then decreased to approximately their original values when the temperature was raised to 125° C.

Principal stress circles determined using the Hoek and Brown failure criterion can be used to generate Mohr failure envelopes for these tests (Hoek and Brown, 1980; Lau and Gorski, 1989). Hoek (1990) also suggests the use of the following equations to determine the equivalent values for the Mohr-Coulomb friction angle, ϕ, and cohesive strength, c.

$$\sigma_n = \sigma_3 + \frac{(\sigma_1 - \sigma_3)^2}{2(\sigma_1 - \sigma_3) + \frac{1}{2}m\sigma_c} \tag{11}$$

where σ_n = normal stress

$$\tau = (\sigma_n - \sigma_3)\sqrt{1 + \frac{m\sigma_c}{2(\sigma_1 - \sigma_3)}} \tag{12}$$

where τ = shear stress

$$\phi = 90 - arcsin\left(\frac{2\tau}{\sigma_1 - \sigma_3}\right) \tag{13}$$

$$c = \tau - \sigma_n tan\phi \tag{14}$$

Mohr-Coulomb friction angles and cohesive strengths, computed by using Equations 11 to 14, are presented in Table 7. The friction angle was found to decrease but the cohesive strength to increase with increasing confining pressure. Temperatures up to 125° C appeared to have no effect on both the friction angle and the cohesive strength of the rock.

CONCLUSIONS

The results of these tests have provided some thermo-mechanical data as well as some insight into the behaviour of the core samples of grey granite from boreholes, drilled in the southwest/subhorizontal (trend/plunge) direction, at the southwest side of Room 209 at the 240 level of the URL. The results also show that temperatures up to 125° C had little effect on the strength and deformability of the rock. Small reductions in failure deviator stress, axial strain at failure and modulus values were observed mostly under the unconfined condition. From the results, the following conclusions can be made.

The failure deviator stress increased as the confining pressure increased. Temperatures up to 125° C appeared to have little effect on the failure deviator stress. Net reductions of 2.3, 0.6 and 1.3% were observed under the unconfined condition and at the confining pressures of 3.5 and 35 MPa respectively, when the temperature was raised from room temperature to 125° C. No change was observed at the confining pressure of 17 MPa. The largest reduction (3.3%) was recorded at the confining pressure of 35 MPa when the temperature was increased from 21° to 75° C.

The axial strain at failure increased with increasing confining pressure. Temperatures up to 125° C appeared to have little effect on the axial strain, except under the unconfined condition. Under the unconfined condition, a reduction of 8.5% was observed at the temperature of 125° C. At the confining pressures of 3.5, 17 and 35 MPa, the mean axial strain decreased by only 1.7, 2.9 and 1.9% respectively when the temperature was raised to 125° C.

At stress levels below approximately 60% of the failure deviator stress, the tangent Young's modulus and the pseudo Young's modulus increased as the confining pressure increased. The increase was particularly pronounced at low confining pressures and at low stress levels. At stress levels above 60% of the failure deviator stress, the confining pressure appeared to have no effect on the moduli. Temperatures up to 125° C were found to have very little effect on both the tangent modulus and the pseudo modulus.

About 3% reduction in the mean modulus values was observed only under the unconfined condition and at the confining pressure of 17 MPa.

The strength properties of the rock specimens are expressed in terms of the Hoek and Brown failure criterion. The predicted uniaxial compressive strength of the intact rock material, σ_c, was found to increase, and then decrease, and the material constant, m, was found to decrease, and then increase as the temperature was raised from 21° to 75° and then to 125° C. The net reductions at 125° C was negligible. The Hoek and Brown failure envelopes derived from these tests show only small reduction in strength at the temperature of 75° C.

No reduction in the uniaxial compressive strength of the rock mass, σ_{cmass}, and in the uniaxial tensile strength of the rock mass, σ_{tmass}, determined by using equations suggested by Hoek, was found as a result of heating the rock up to 125° C.

Mohr-Coulomb friction angles and cohesive strengths of the rock were computed by using equations suggested by Hoek. The friction angle, ϕ, decreased and the cohesive strength, c, increased with increasing confining pressure. Both ϕ and c appeared not to be affected by heating up to 125° C.

The results of these tests affirm that core samples of the grey granite drilled at the southwest side of Room 209 and in the southwest/subhorizontal (trend/plunge) direction have lower wave velocities, lower strength and lower modulus values than those drilled at the northeast side of Room 209 and in the northeast/subhorizontal direction, suggesting that more microcracks are present in the samples obtained from the southwest side of Room 209.

RECOMMENDATIONS

One of the main rock mechanics issues related to the construction and operation of the URL is experimentally identifying the temperature-dependent strength and deformation characteristics of the host rock. This high temperature uniaxial and triaxial compression testing program has addressed this issue and is recommended for the URL characterization program during the operating phase of the URL and for any future site selection program if the disposal concept is deemed acceptable.

Ambient room temperature and high temperature tension tests should also be included in the testing program in order to obtain more accurate values of σ_c and m in the Hoek and Brown failure criterion.

Although results obtained from this testing program have shed some light on the thermo-mechanical properties of the URL rock samples, some questions remain to be answered. What are the scale effects on the thermo-mechanical properties of the URL rock samples? What are the effects of moisture on the thermo-mechanical properties? Will the rock behave the same way at very high confining pressure? These questions should be addressed in the future.

Core samples from boreholes drilled at the northeast side of Room 209 were found to be consistently stronger and stiffer than those from the southwest side of Room 209. One reason for this behaviour is that more microcracks were present in the core samples from the southwest side. Is this related to the stress distribution around the URL excavation, or is this due to the local differences in rock properties? These questions should also be addressed.

ACKNOWLEDGEMENTS

The authors wish to express their thanks to R. Jackson of CANMET for reviewing this report and making several helpful suggestions. Gratitude is expressed to J. Folta of CANMET for the preparation of specimens and for carrying out the compression wave and shear wave velocities measurements on the specimens.

REFERENCES

Brown, E.T. (1981), "Rock characterization testing and monitoring, ISRM suggested methods", International Society for Rock Mechanics, the Commission on Testing Methods, Pergamon, 211 p.

Gorski, B. (1987), "Post-failure uniaxial strength determinations using a servo-hydraulic test system", Division Report MRL 87-33(INT), CANMET, Energy, Mines and Resources Canada, 77 p.

Gyenge, M. and Herget, G. (1977), "Pit slope manual supplement 3-2 - laboratory tests for design parameters", CANMET, Report 77-26, 74 p.

Gyenge, M. and Ladanyi, B. (1977), "Pit slope manual supplement 3-5 - sampling and specimen preparation", CANMET, Report 77-29, 30 p.

Hoek, E. (1990), "Estimating Mohr-Coulomb friction and cohesion values from the Hoek-Brown failure criterion", Int. J. Rock Mech. Min. Sci. & Geomech. Abstr., Vol. 27, No. 3, p. 227-229.

Hoek, E. and Brown, E.T. (1980), "Underground excavations in rock", The institution of Mining and Metallurgy, London, 527 p.

Lau, J.S.O., Jackson, R. and Gorski, B. (1988), "High temperature triaxial tests on rock samples from boreholes 209-021-SV1 and 209-030-DIL1, Lac du Bonnet, Manitoba", Division Report MRL 88-112(TR), CANMET, Energy, Mines and Resources Canada, 57 p.

Lau, J.S.O. and Gorski, B. (1989), "High temperature uniaxial compression tests on URL rock samples from boreholes 209-021-SV1 and 209-030-DIL1", Divisional Report MRL 89-90(TR), CANMET, Energy, Mines and Resources Canada, 68 p.

Lau, J.S.O. and Gorski, B. (1990), "High temperature uniaxial and triaxial compression tests on URL rock samples from boreholes 209-021-SV1 and 209-025-SV2", Divisional Report MRL 90-079(TR), CANMET, Energy, Mines and Resources Canada, 46 p.

MTS Systems Corporation (1986), "Operation manual for 815 rock mechanics test systems", MTS Systems Corp., Minneapolis, Minnesota, U.S.A.

Table 1. Dimensions, densities and dynamic elastic properties of rock specimens.

Specimen identification	Length (mm)	Diameter (mm)	Bulk density (Mg/m^3)	P-wave velocity (km/s)	S-wave velocity (km/s)	Dynamic Young's modulus (GPa)	Dynamic shear modulus (GPa)	Dynamic Poisson's ratio
209-030-DIL1-0.784	109.51	44.97	2.64	4.525	2.711	47.34	19.40	0.22
209-030-DIL1-0.906	109.66	44.96	2.64	4.476	2.681	46.31	18.98	0.22
209-030-DIL1-2.44	107.94	44.96	2.63	4.687	2.763	49.55	20.08	0.23
209-030-DIL1-2.55	107.28	45.00	2.63	4.668	2.751	49.13	19.91	0.23
209-030-DIL1-2.66	105.64	44.89	2.64	4.828	2.740	50.03	19.81	0.26
209-030-DIL1-2.77	109.29	44.87	2.64	4.505	2.677	46.44	18.92	0.23
209-030-DIL1-2.89	111.96	45.06	2.62	4.742	2.775	50.03	20.18	0.24
209-030-DIL1-3.092	110.22	44.84	2.63	4.305	2.643	44.01	18.37	0.20
209-030-DIL1-3.57	108.84	44.92	2.63	4.531	2.632	45.37	18.21	0.25
209-030-DIL1-3.69	108.22	44.88	2.63	4.448	2.615	44.46	17.99	0.24
209-030-DIL1-3.80	104.44	44.88	2.63	4.636	2.674	47.03	18.80	0.25
209-030-DIL1-8.30	104.67	44.94	2.64	4.367	2.652	44.83	18.56	0.21
209-030-DIL1-8.60	98.58	44.86	2.65	4.467	2.525	42.71	16.88	0.27
209-030-DIL1-9.60	102.44	44.94	2.64	4.402	2.655	45.18	18.60	0.21
209-030-DIL1-9.70	105.46	44.98	2.63	4.503	2.647	45.57	18.44	0.24
209-030-DIL1-9.90	102.36	44.98	2.64	4.535	2.680	46.68	18.95	0.23
209-018-EXT4-5.161	107.97	44.94	2.63	4.319	2.699	45.20	19.16	0.18
209-018-EXT4-5.275	108.32	44.95	2.63	4.150	2.591	41.70	17.66	0.18
209-018-EXT4-5.390	107.14	44.95	2.63	4.202	2.527	40.86	16.79	0.22
209-018-EXT4-5.505	111.90	44.95	2.63	4.114	2.602	41.55	17.81	0.17
209-018-EXT4-6.605	110.61	44.94	2.65	4.571	2.772	49.24	20.37	0.21
209-018-EXT4-6.720	109.77	44.94	2.64	4.127	2.407	38.00	15.30	0.24
209-018-EXT4-6.835	109.30	44.94	2.64	4.220	2.424	38.89	15.51	0.25
209-018-EXT4-6.949	109.43	44.93	2.64	4.225	2.459	39.72	15.96	0.24
209-018-EXT4-7.075	114.05	44.92	2.65	4.544	2.722	47.91	19.63	0.22
209-018-EXT4-7.189	109.31	44.90	2.64	4.204	2.397	38.20	15.17	0.26
209-018-EXT4-7.425	116.10	44.90	2.66	4.237	2.470	40.34	16.23	0.24
209-018-EXT4-7.654	107.99	44.90	2.63	4.122	2.571	41.08	17.39	0.18
209-018-EXT4-8.220	111.41	44.90	2.63	4.111	2.504	39.74	16.48	0.21
209-018-EXT4-8.334	108.60	44.90	2.63	4.098	2.371	36.92	14.79	0.25
209-018-EXT4-8.450	110.66	44.90	2.63	4.224	2.370	37.52	14.77	0.27
209-018-EXT4-8.905	101.32	44.91	2.63	4.136	2.514	40.13	16.62	0.21
209-018-EXT4-9.035	106.58	44.92	2.63	4.115	2.520	40.08	16.70	0.20
209-018-EXT4-9.216	112.83	44.91	2.64	4.073	2.464	38.83	16.02	0.21
209-018-EXT4-9.442	105.10	44.91	2.64	3.936	2.367	36.00	14.79	0.22
209-018-EXT4-9.555	103.97	44.92	2.63	4.014	2.368	36.38	14.75	0.23
209-018-EXT4-9.667	105.86	44.94	2.63	4.010	2.428	37.54	15.50	0.21
209-018-EXT4-9.779	102.09	44.94	2.63	3.882	2.331	34.81	14.29	0.22
209-018-EXT4-9.891	110.56	44.94	2.63	4.236	2.441	39.21	15.67	0.25
209-018-EXT4-10.700	108.91	44.96	2.63	4.205	2.487	40.04	16.26	0.23
209-018-EXT4-10.922	107.36	44.97	2.63	4.227	2.365	37.42	14.71	0.27
Mean			2.64	4.315	2.561	42.49	17.33	0.23
Standard deviation			0.01	0.233	0.137	4.42	1.85	0.03

Table 2. Results of ambient and high temperature uniaxial and triaxial compression tests.

Specimen Identification	Confining Pressure (MPa)	Temp. (deg C.)	Total Axial Strain (%)	Failure Deviator Stress (MPa)	Tangent Young's Modulus (GPa)	Pseudo Young's Modulus (GPa)	Poisson's Ratio	θ (deg.)	Failure characteristics
209-030-DIL1-2.44*	0.0	25	0.333	145	54.58	53.08	0.32		multiple cracks, wedge-shaped bottom end
209-030-DIL1-2.77	0.0	25	0.341	171	62.45	61.51	0.28		multiple vertical cracks
209-030-DIL1-2.89	0.0	25	0.333	160	59.84	58.68	0.31		multiple cracks, wedge-shaped bottom end
209-030-DIL1-3.57	0.0	25	0.408	175	61.52	60.41	0.29		multiple vertical cracks
209-018-EXT4-5.275	0.0	21	0.339	165	65.63	64.60	0.22		multiple vertical cracks
209-030-DIL1-2.55	0.0	75	0.334	167	61.27	60.25	0.24		multiple vertical cracks
209-030-DIL1-3.69	0.0	75	0.323	169	62.38	61.36	0.25		multiple vertical cracks
209-018-EXT4-5.161	0.0	75	0.317	162	65.62	64.28			multiple cracks
209-030-DIL1-2.66	0.0	125	0.325	163	60.55	59.45	0.26		multiple vertical cracks
209-030-DIL1-3.80	0.0	125	0.326	161	57.54	56.11	0.24		multiple cracks, top wedge
209-018-EXT4-10.922	0.0	125	0.324	168	64.25	63.02			multiple cracks
209-030-DIL1-0.784	3.5	21	0.422	232	68.62	68.78	0.27		multiple cracks, wedge-shaped bottom end
209-018-EXT4-5.505	3.5	21	0.395	220	68.88	68.60	0.27	70	2 fragments, irregular fracture
209-018-EXT4-8.905	3.5	21	0.434	237	68.68	68.52	0.30	66	2 fragments, curved fracture
209-018-EXT4-6.605	3.5	75	0.387	237	75.43	75.52	0.33		multiple cracks, wedge-shaped bottom end
209-018-EXT4-7.189	3.5	75	0.401	235	71.95	71.85	0.27	68	3 fragments, fracture, wedge-shaped bottom end
209-018-EXT4-9.667	3.5	75	0.410	228	69.04	68.92	0.31		2 fragments, wedge-shaped bottom end
209-030-DIL1-9.60	3.5	125	0.440	239	67.58	67.23		67	3 fragments, shear fracture, wedge-shaped top end
209-018-EXT4-6.720	3.5	125	0.391	223	69.94	69.80	0.32	67	3 fragments, fracture, wedge-shaped top end
209-018-EXT4-9.035	3.5	125	0.399	223	68.21	67.95	0.25	68	3 fragments, fracture, wedge-shaped bottom end

*results rejected due to the incompatibility of the failure deviator stress with the rest

Table 2 - (Cont'd)

Specimen Identification	Confining Pressure (MPa)	Temp. (deg C.)	Total Axial Strain (%)	Failure Deviator Stress (MPa)	Tangent Young's Modulus (GPa)	Pseudo Young's Modulus (GPa)	Poisson's Ratio	θ (deg.)	Failure characteristics
209-030-DIL1-0.906	17.0	21	0.656	366	69.34	70.45	0.34	65	2 fragments, irregular fracture
209-018-EXT4-6.835	17.0	21	0.602	366	72.16	73.38	0.35	70	2 fragments, curved fracture
209-018-EXT4-9.216	17.0	21	0.621	373	71.05	72.11	0.38	57	2 fragments, fracture
209-030-DIL1-8.30	17.0	75	0.639	379	67.68	68.70		60	3 fragments, fracture, wedge-shaped top end
209-018-EXT4-6.949	17.0	75	0.601	367	71.22	72.34	0.36	69	2 fragments, curved fracture
209-018-EXT4-9.442	17.0	75	0.606	359	69.47	70.57	0.36	69	2 fragments, curved fracture
209-030-DIL1-9.70	17.0	125	0.606	379	69.87	70.18		60	4 fragments, fracture, wedge-shaped top and bottom ends
209-018-EXT4-7.425*	17.0	125	0.541	326	72.83	74.08	0.31	60	2 fragments, fracture
209-018-EXT4-8.334	17.0	125	0.624	359	66.09	66.99	0.27	65	2 fragments, curved fracture
209-018-EXT4-9.779	17.0	125	0.595	366	70.54	71.57	0.33	68	2 fragments, curved fracture
209-031-DIL1-3.092	35.0	21	0.785	490	70.40	71.98	0.34	68	2 fragments, planar fracture
209-018-EXT4-7.654	35.0	21	0.792	503	71.22	72.68	0.36	56	2 fragments, irregular fracture
209-018-EXT4-9.891	35.0	21	0.790	498	72.19	73.82	0.36	70	2 fragments, fracture
209-030-DIL1-8.60	35.0	75	0.790	488	69.64	71.03		68	2 fragments, shear fracture
209-018-EXT4-5.390	35.0	75	0.768	478	70.55	71.99	0.36	63	2 fragments, fracture
209-018-EXT4-8.450	35.0	75	0.744	476	70.52	71.78	0.34	70	3 fragments, fracture, wedge-shaped bottom end
209-018-EXT4-9.555*	35.0	75	0.723	449	69.04	70.50	0.38	70	3 fragments, fracture, wedge-shaped bottom end
209-030-DIL1-9.90	35.0	125	0.806	496	68.39	69.75		68	2 fragments, unconnected and stepped fracture
209-018-EXT4-7.075	35.0	125	0.759	502	74.44	75.95	0.27	60	2 fragments, fracture
209-018-EXT4-8.220	35.0	125	0.756	474	71.32	72.66	0.36	65	2 fragments, curved fracture
209-018-EXT4-10.700*	35.0	125	0.568	266	73.85	74.67	0.32		2 fragments, wedge-shaped bottom end

*results rejected due to the incompatibility of the failure deviator stress with the rest

Table 3. Tangent Young's moduli at stress levels ranging from 10 to 90 % of the failure deviator stress.

Specimen Identification	σ_3 (MPa)	Temp. (deg C.)	Tangent Young's Modulus (GPa)								
			10 %	20 %	30 %	40 %	50 %	60 %	70 %	80 %	90 %
209-030-DIL1-2.44*	0.0	25	27.82	39.19	46.33	51.28	54.58	56.12	56.08	54.47	48.38
209-030-DIL1-2.77	0.0	25	36.05	49.04	56.27	60.31	62.45	63.04	62.14	59.66	52.69
209-030-DIL1-2.89	0.0	25	32.71	45.33	52.70	57.25	59.84	60.81	60.28	58.19	51.94
209-030-DIL1-3.57	0.0	25	31.76	45.47	53.96	58.96	61.52	62.06	60.62	57.01	49.00
209-018-EXT4-5.275	0.0	21	37.84	51.76	58.88	63.28	65.63	66.23	65.13	62.23	56.24
209-030-DIL1-2.55	0.0	75	35.99	48.38	55.13	59.00	61.27	62.17	61.79	60.08	54.92
209-030-DIL1-3.69	0.0	75	37.73	49.43	55.96	60.07	62.38	63.12	62.39	60.10	54.60
209-018-EXT4-5.161	0.0	75	35.96	49.77	57.70	62.67	65.62	66.89	66.61	64.76	56.19
209-030-DIL1-2.66	0.0	125	34.63	46.65	53.72	58.08	60.55	61.45	60.85	58.70	53.10
209-030-DIL1-3.80	0.0	125	37.21	46.36	50.94	54.59	57.54	59.91	61.78	63.21	57.36
209-018-EXT4-10.922	0.0	125	35.44	48.52	56.53	61.48	64.25	65.20	64.44	61.88	54.45
209-030-DIL1-0.784	3.5	21	52.05	63.64	67.48	68.72	68.62	67.19	64.29	59.66	51.64
209-018-EXT4-5.505	3.5	21	52.10	60.29	65.27	68.02	68.88	67.95	65.12	60.04	51.10
209-018-EXT4-8.905	3.5	21	52.82	60.70	65.51	68.06	68.68	67.43	64.19	58.49	48.76
209-018-EXT4-6.605	3.5	75	63.21	69.59	73.44	75.32	75.43	73.77	70.17	64.20	54.25
209-018-EXT4-7.189	3.5	75	56.99	64.90	69.19	71.45	71.95	70.74	67.69	62.43	53.34
209-018 EXT4-9.667	3.5	75	52.97	61.51	66.08	68.49	69.04	67.80	64.61	59.07	49.50
209-030-DIL1-9.60	3.5	125	50.44	58.89	63.81	66.59	67.58	66.87	64.40	59.87	49.39
209-018-EXT4-6.720	3.5	125	54.52	62.54	67.00	69.38	69.94	68.75	65.67	60.33	51.03
209-018-EXT4-9.035	3.5	125	52.22	60.38	64.91	67.42	68.21	67.34	64.73	60.09	51.72

*results rejected due to the incompatibility of the failure deviator stress with the rest

Table 3 - (Cont'd)

Specimen Identification	σ_3 (MPa)	Temp. (deg C.)	Tangent Young's Modulus (GPa)								
			10 %	20 %	30 %	40 %	50 %	60 %	70 %	80 %	90 %
209-030-DIL1-0.906	17.0	21	71.83	72.92	72.60	71.42	69.34	66.22	61.87	55.92	47.27
209-018-EXT4-6.835	17.0	21	75.06	76.15	75.75	74.45	72.16	68.77	64.04	57.55	47.96
209-018-EXT4-9.216	17.0	21	72.30	73.97	73.97	73.01	71.05	67.97	63.55	57.38	48.22
209-030-DIL1-8.30	17.0	75	70.15	71.01	70.68	69.59	67.68	64.86	60.96	55.70	48.10
209-018-EXT4-6.949	17.0	75	73.55	74.43	74.34	73.29	71.22	68.00	63.40	57.00	47.46
209-018-EXT4-9.442	17.0	75	71.60	72.77	72.60	71.52	69.47	66.32	61.87	55.71	46.52
209-030-DIL1-9.70	17.0	125	78.21	72.75	70.03	70.22	69.87	67.81	63.82	57.35	47.06
209-018-EXT4-7.425*	17.0	125	77.03	76.36	76.29	75.13	72.83	69.22	64.02	56.66	45.22
209-018-EXT4-8.334	17.0	125	67.26	68.44	68.52	67.75	66.09	63.43	59.62	54.33	46.44
209-018-EXT4-9.779	17.0	125	72.29	73.38	73.38	72.45	70.54	67.53	63.24	57.26	48.47
209-030-DIL1-3.092	35.0	21	79.30	77.92	75.96	73.47	70.40	66.63	62.00	56.26	48.46
209-018-EXT4-7.654	35.0	21	79.13	78.07	76.32	74.06	71.22	67.72	63.41	58.06	50.81
209-018-EXT4-9.891	35.0	21	81.69	80.23	78.03	75.37	72.19	68.39	63.84	58.32	50.95
209-030-DIL1-8.60	35.0	75	76.83	75.94	74.41	72.33	69.64	66.23	61.95	56.56	49.05
209-018-EXT4-5.390	35.0	75	78.09	76.99	75.46	73.34	70.55	66.99	62.49	56.76	48.72
209-018-EXT4-8.450	35.0	75	77.09	75.91	74.72	72.94	70.52	67.37	63.34	58.21	51.06
209-018-EXT4-9.555*	35.0	75	77.04	75.77	74.09	71.87	69.04	65.51	61.11	55.59	47.70
209-030-DIL1-9.90	35.0	125	75.13	74.27	72.95	71.02	68.39	64.96	60.55	54.86	47.08
209-018-EXT4-7.075	35.0	125	82.33	81.13	79.56	77.36	74.44	70.69	65.93	59.85	51.44
209-018-EXT4-8.220	35.0	125	76.52	76.44	75.55	73.87	71.32	67.77	63.01	56.64	47.56
209-018-EXT4-10.700*	35.0	125	65.49	71.23	74.30	75.14	73.85	70.26	63.85	53.31	36.77

*results rejected due to the incompatibility of the failure deviator stress with the rest

Table 4. Pseudo Young's moduli at stress levels ranging from 10 to 90 % of the failure deviator stress.

Specimen Identification	σ_3 (MPa)	Temp. (deg C.)	Pseudo Young's Modulus (GPa)								
			10 %	20 %	30 %	40 %	50 %	60 %	70 %	80 %	90 %
209-030-DIL1-2.44*	0.0	25	18.79	33.72	42.89	48.92	53.08	55.49	56.23	55.41	52.02
209-030-DIL1-2.77	0.0	25	24.35	42.92	52.90	58.47	61.51	62.87	62.71	61.03	56.98
209-030-DIL1-2.89	0.0	25	21.81	39.33	49.22	55.14	58.68	60.45	60.67	59.37	55.71
209-030-DIL1-3.57	0.0	25	17.95	38.61	49.96	56.65	60.41	61.95	61.50	58.99	53.60
209-018-EXT4-5.275	0.0	21	18.40	44.86	55.52	61.25	64.60	66.07	65.82	63.83	59.75
209-030-DIL1-2.55	0.0	75	25.55	42.57	52.01	57.19	60.25	61.83	62.09	61.05	58.30
209-030-DIL1-3.69	0.0	75	27.46	44.03	52.87	58.16	61.36	62.87	62.88	61.38	57.80
209-018-EXT4-5.161	0.0	75	24.62	43.22	53.96	60.34	64.28	66.38	66.88	65.82	61.62
209-030-DIL1-2.66	0.0	125	26.09	40.94	50.38	56.05	59.45	61.12	61.27	59.91	56.57
209-030-DIL1-3.80	0.0	125	29.48	42.30	48.70	52.81	56.11	58.76	60.88	62.53	61.71
209-018-EXT4-10.922	0.0	125	25.91	42.23	52.74	59.18	63.02	64.87	64.97	63.31	58.95
209-030-DIL1-0.784	3.5	21	37.33	58.51	65.99	68.21	68.78	68.02	65.86	62.11	56.19
209-018-EXT4-5.505	3.5	21	37.06	56.47	62.95	66.80	68.60	68.56	66.69	62.76	56.04
209-018-EXT4-8.905	3.5	21	40.41	56.99	63.29	66.94	68.52	68.21	65.98	61.53	54.05
209-018-EXT4-6.605	3.5	75	48.95	66.62	71.68	74.53	75.52	74.74	72.13	67.37	59.69
209-018-EXT4-7.189	3.5	75	43.73	61.52	67.21	70.47	71.85	71.49	69.37	65.23	58.40
209-018 EXT4-9.667	3.5	75	39.13	57.84	63.97	67.44	68.92	68.57	66.37	62.03	54.76
209-030-DIL1-9.60	3.5	125	43.28	54.99	61.52	65.35	67.23	67.36	65.78	62.30	55.41
209-018-EXT4-6.720	3.5	125	44.20	59.02	64.94	68.34	69.80	69.49	67.36	63.18	56.18
209-018-EXT4-9.035	3.5	125	40.16	56.83	62.81	66.31	67.95	67.91	66.18	62.57	56.45

*results rejected due to the incompatibility of the failure deviator stress with the rest

Table 4 - (Cont'd)

Specimen Identification	σ_3 (MPa)	Temp. (deg C.)	Pseudo Young's Modulus (GPa)								
			10 %	20 %	30 %	40 %	50 %	60 %	70 %	80 %	90 %
209-030-DIL1-0.906	17.0	21	65.49	72.69	72.83	72.08	70.45	67.86	64.14	59.00	51.88
209-018-EXT4-6.835	17.0	21	68.28	75.93	76.03	75.18	73.38	70.55	66.50	60.91	53.08
209-018-EXT4-9.216	17.0	21	63.97	73.51	74.05	73.57	72.11	69.60	65.86	60.58	53.13
209-030-DIL1-8.30	17.0	75	63.96	70.83	70.91	70.20	68.70	66.34	62.99	58.42	52.18
209-018-EXT4-6.949	17.0	75	72.69	74.08	74.47	73.90	72.34	69.70	65.80	60.32	52.55
209-018-EXT4-9.442	17.0	75	67.75	72.44	72.76	72.14	70.57	67.98	64.19	58.90	51.44
209-030-DIL1-9.70	17.0	125	81.37	75.25	71.13	69.95	70.18	68.98	65.97	60.77	52.46
209-018-EXT4-7.425*	17.0	125	81.46	76.19	76.41	75.80	74.08	71.13	66.74	60.48	51.33
209-018-EXT4-8.334	17.0	125	64.69	68.02	68.55	68.21	66.99	64.84	61.62	57.08	50.71
209-018-EXT4-9.779	17.0	125	70.09	72.98	73.46	72.99	71.57	69.12	65.48	60.36	53.16
209-030-DIL1-3.092	35.0	21	78.68	78.70	76.98	74.75	71.98	68.56	64.37	59.19	52.62
209-018-EXT4-7.654	35.0	21	77.13	78.73	77.23	75.23	72.68	69.52	65.62	60.80	54.71
209-018-EXT4-9.891	35.0	21	79.12	81.13	79.16	76.73	73.82	70.33	66.16	61.13	54.90
209-030-DIL1-8.60	35.0	75	75.97	76.47	75.21	73.41	71.03	67.98	64.14	59.32	53.10
209-018-EXT4-5.390	35.0	75	79.12	77.53	76.27	74.45	71.99	68.83	64.80	59.70	53.05
209-018-EXT4-8.450	35.0	75	80.06	76.33	75.36	73.88	71.78	69.00	65.42	60.85	54.91
209-018-EXT4-9.555*	35.0	75	77.77	76.42	74.97	73.02	70.50	67.32	63.36	58.42	52.01
209-030-DIL1-9.90	35.0	125	76.43	74.69	73.66	72.03	69.75	66.73	62.82	57.78	51.17
209-018-EXT4-7.075	35.0	125	84.68	81.68	80.40	78.51	75.95	72.62	68.37	62.97	55.92
209-018-EXT4-8.220	35.0	125	75.97	76.56	76.05	74.77	72.66	69.62	65.48	59.93	52.35
209-018-EXT4-10.700*	35.0	125	84.22	68.57	72.95	74.90	74.67	72.24	67.28	58.87	44.98

*results rejected due the incompatibility of the failure deviator stress with the rest

Table 5. Mean values and standard deviations (in brackets) of failure deviator stress, axial strain at failure, tangent Young's modulus and pseudo Young's modulus.

Confining pressure (MPa)	Temperature (° C)	Mean failure deviator stress (MPa)	Mean failure axial strain (%)	Mean tangent Young's modulus (GPa)	Mean Pseudo Young's modulus (GPa)	Mean Poisson's ratio
0.0	21-25	167.8 (6.6)	0.355 (0.035)	62.36 (2.43)	61.30 (2.49)	0.275 (0.039)
	75	166.0 (3.6)	0.325 (0.009)	63.09 (2.26)	61.96 (2.08)	0.245 (0.007)
	125	164.0 (3.6)	0.325 (0.001)	60.78 (3.36)	59.53 (3.46)	0.250 (0.014)
3.5	21	229.7 (8.7)	0.417 (0.020)	68.73 (0.14)	68.63 (0.13)	0.280 (0.017)
	75	233.3 (4.7)	0.399 (0.012)	72.14 (3.20)	72.10 (3.31)	0.303 (0.031)
	125	228.3 (9.2)	0.410 (0.026)	68.58 (1.22)	68.33 (1.33)	0.285 (0.049)
17.0	21	368.3 (4.0)	0.626 (0.027)	70.85 (1.42)	71.98 (1.47)	0.357 (0.021)
	75	368.3 (10.1)	0.615 (0.021)	69.46 (1.77)	70.54 (1.82)	0.360 (0.000)
	125	368.0 (10.1)	0.608 (0.015)	68.83 (2.40)	69.58 (2.35)	0.300 (0.042)
35.0	21	497.0 (6.6)	0.789 (0.004)	71.27 (0.90)	72.83 (0.93)	0.353 (0.012)
	75	480.7 (6.4)	0.767 (0.023)	70.24 (0.52)	71.60 (0.50)	0.350 (0.014)
	125	490.7 (14.7)	0.774 (0.028)	71.38 (3.03)	72.79 (3.10)	0.315 (0.064)

Table 6. Values of σ_c, m, s, r^2, σ_{cmass} and σ_{tmass} derived from the Hoek and Brown failure criterion.

Test Temperature (°C.)	Number of specimens	σ_c (MPa)	m	s	r^2	σ_{cmass} (MPa)	σ_{tmass} (MPa)
21-25	13	171	36.32	1.00	0.9983	171	4.70
75	12	180	32.09	1.00	0.9948	180	5.60
125	12	172	35.39	1.00	0.9927	172	4.86

Table 7. Values of the Mohr-Coulomb friction angle ϕ and cohesive strength c.

Confining pressure (MPa)	Test temperature (°C)	Number of specimens	ϕ	c (MPa)
0.0	21-25	4	64°	19
	75	3	64°	19
	125	3	65°	19
3.5	21	3	61°	24
	75	3	59°	26
	125	3	60°	24
17.0	21	3	54°	37
	75	3	53°	40
	125	3	54°	37
35.0	21	3	49°	52
	75	3	49°	51
	125	3	49°	51

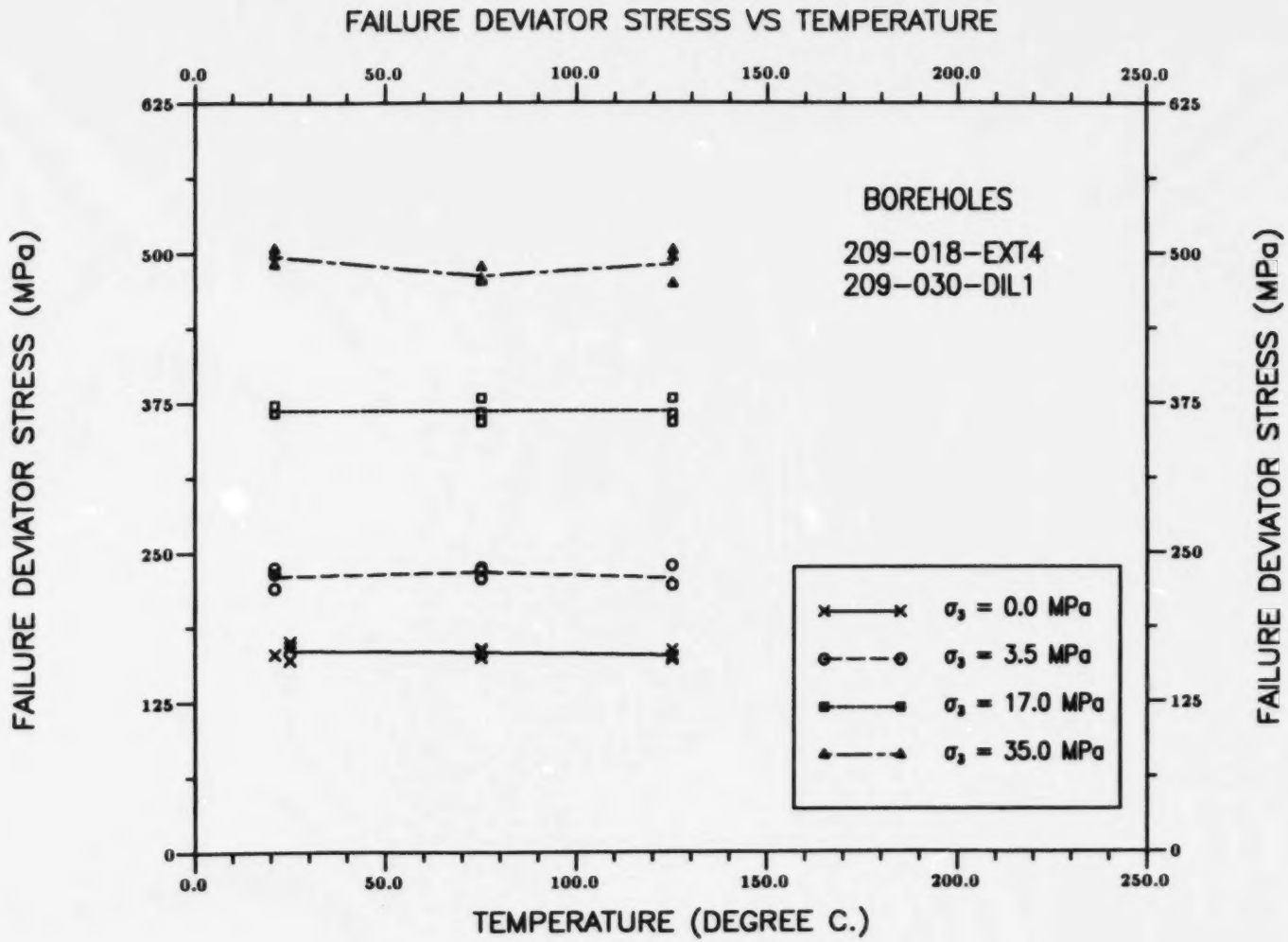

Figure 1. Plots of failure deviator stress versus temperature.

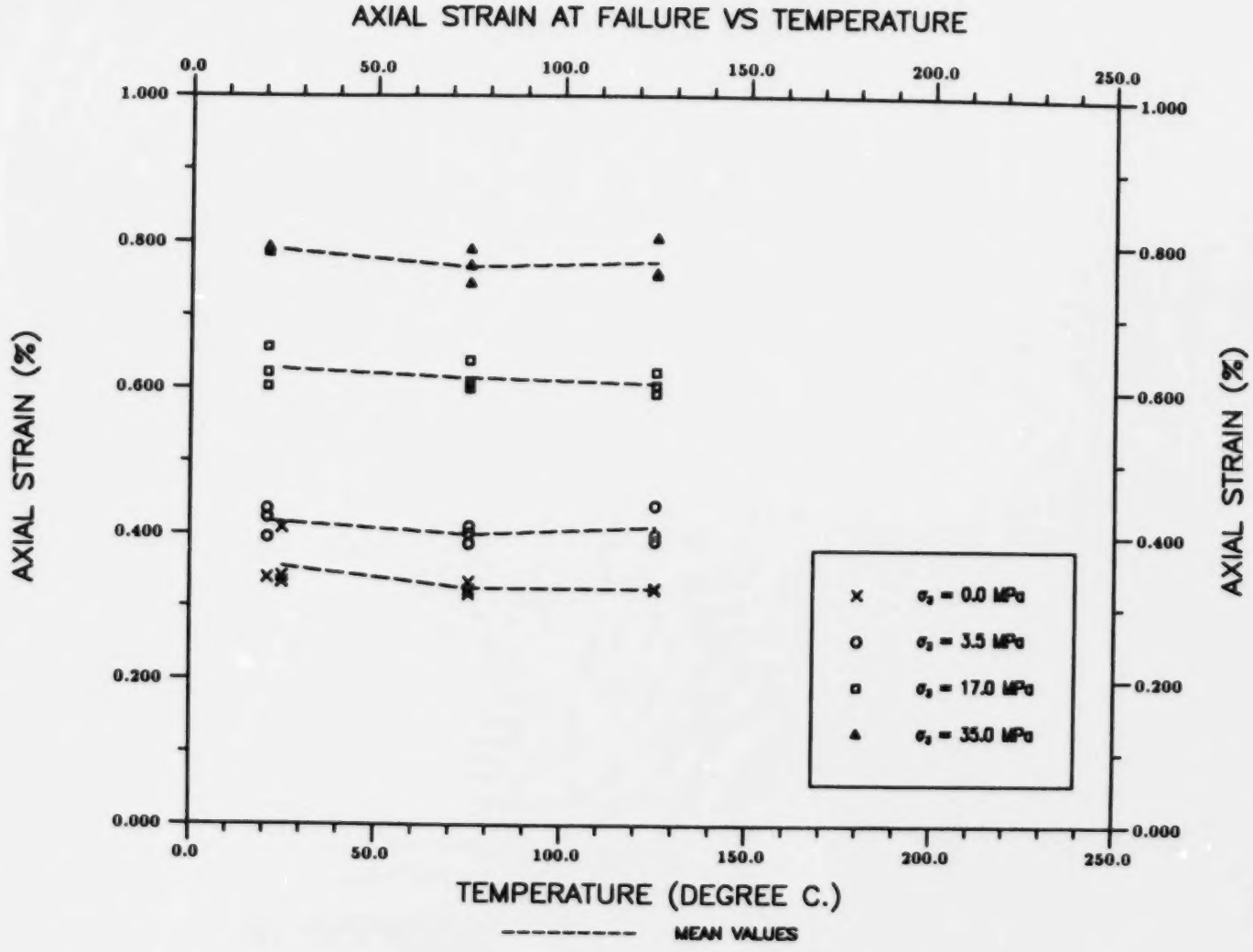

Figure 2. Plots of axial strain at failure versus temperature.

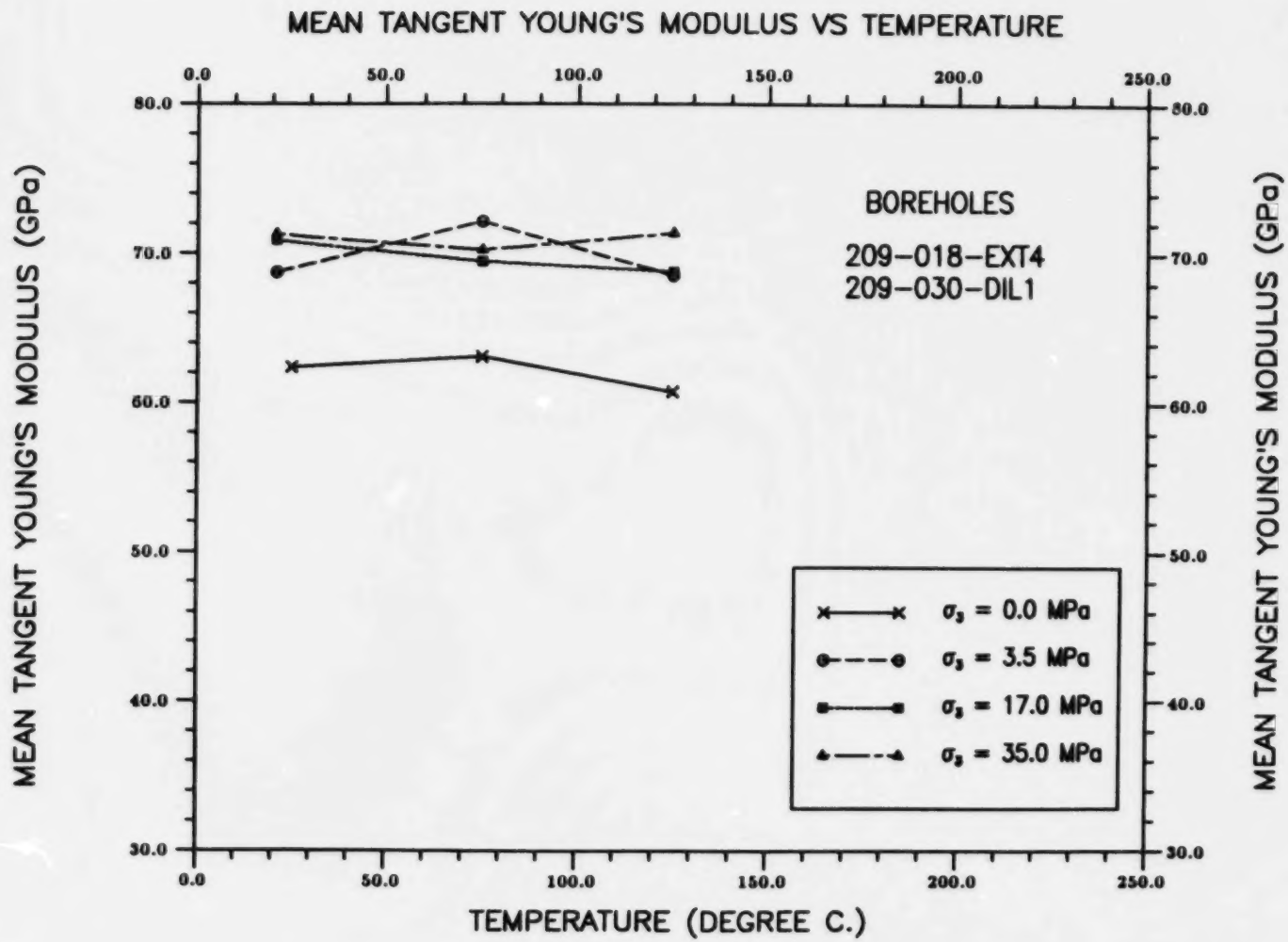

Figure 3. Plots of mean tangent Young's modulus at the stress level of 50 % of $(\sigma_1 - \sigma_3)_f$ versus temperature.

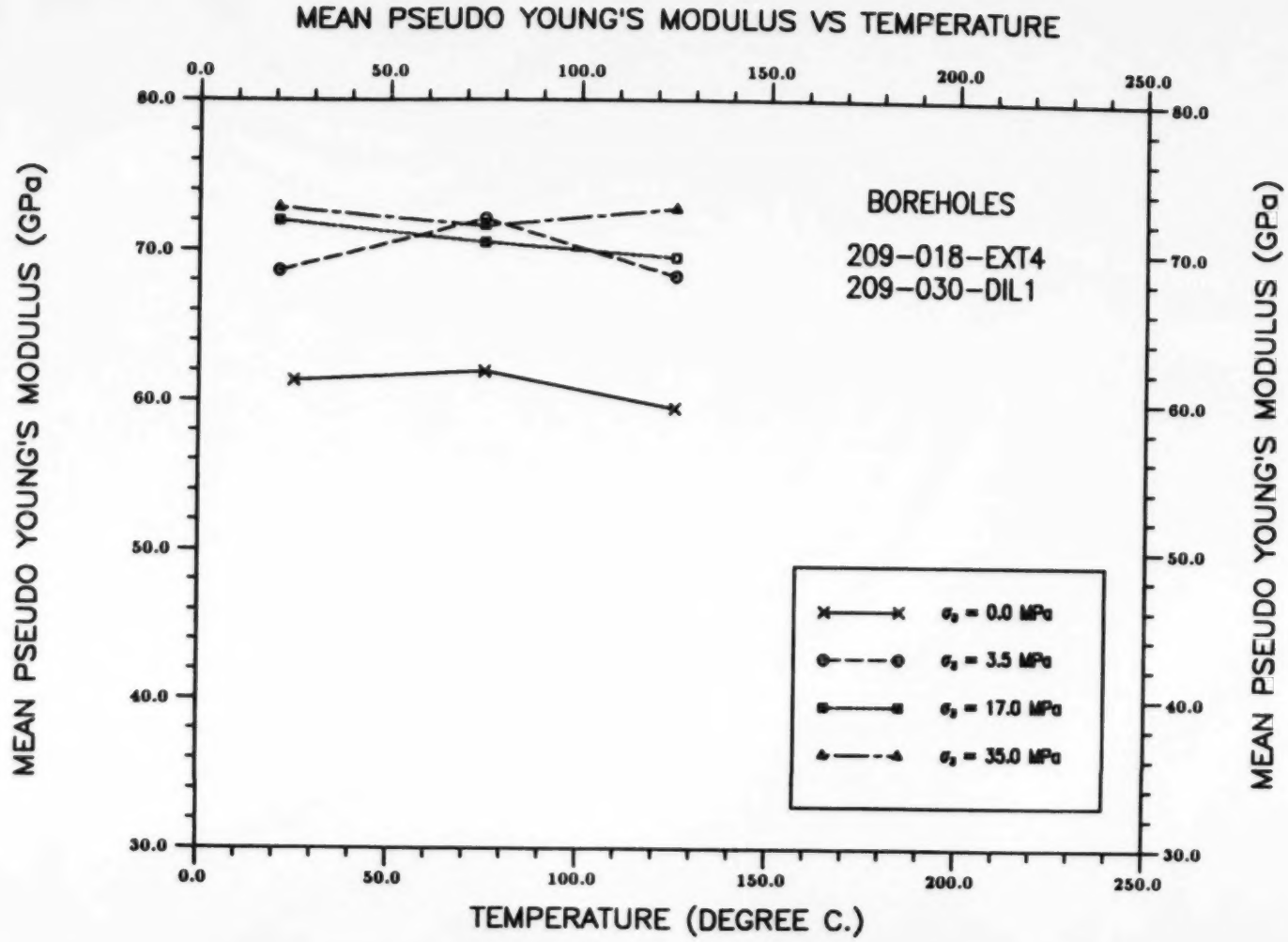

Figure 4. Plots of mean pseudo Young's modulus at the stress level of 50 % of $(\sigma_1 - \sigma_3)_f$ versus temperature.

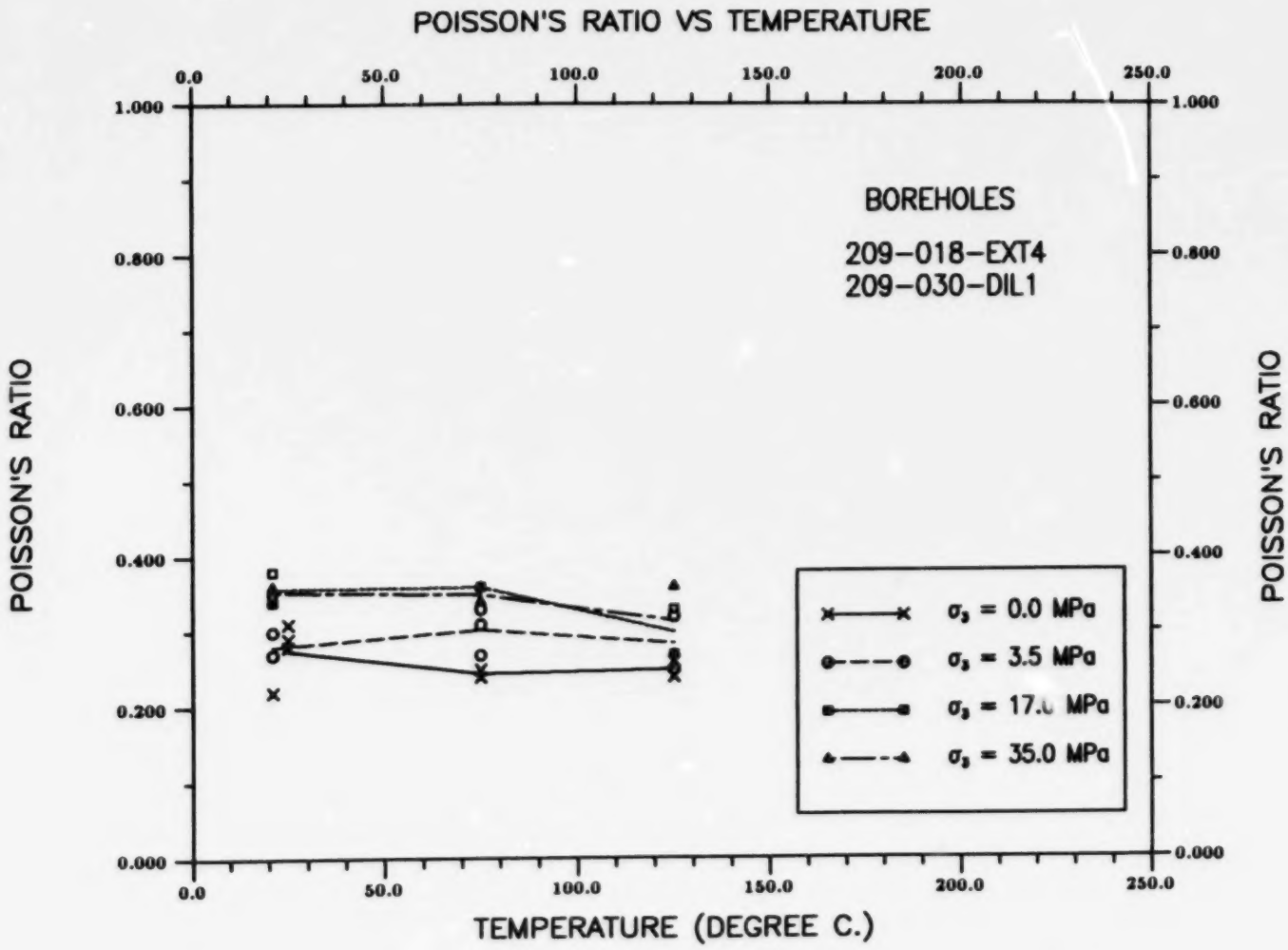

Figure 5. Plots of Poisson's ratio versus temperature.

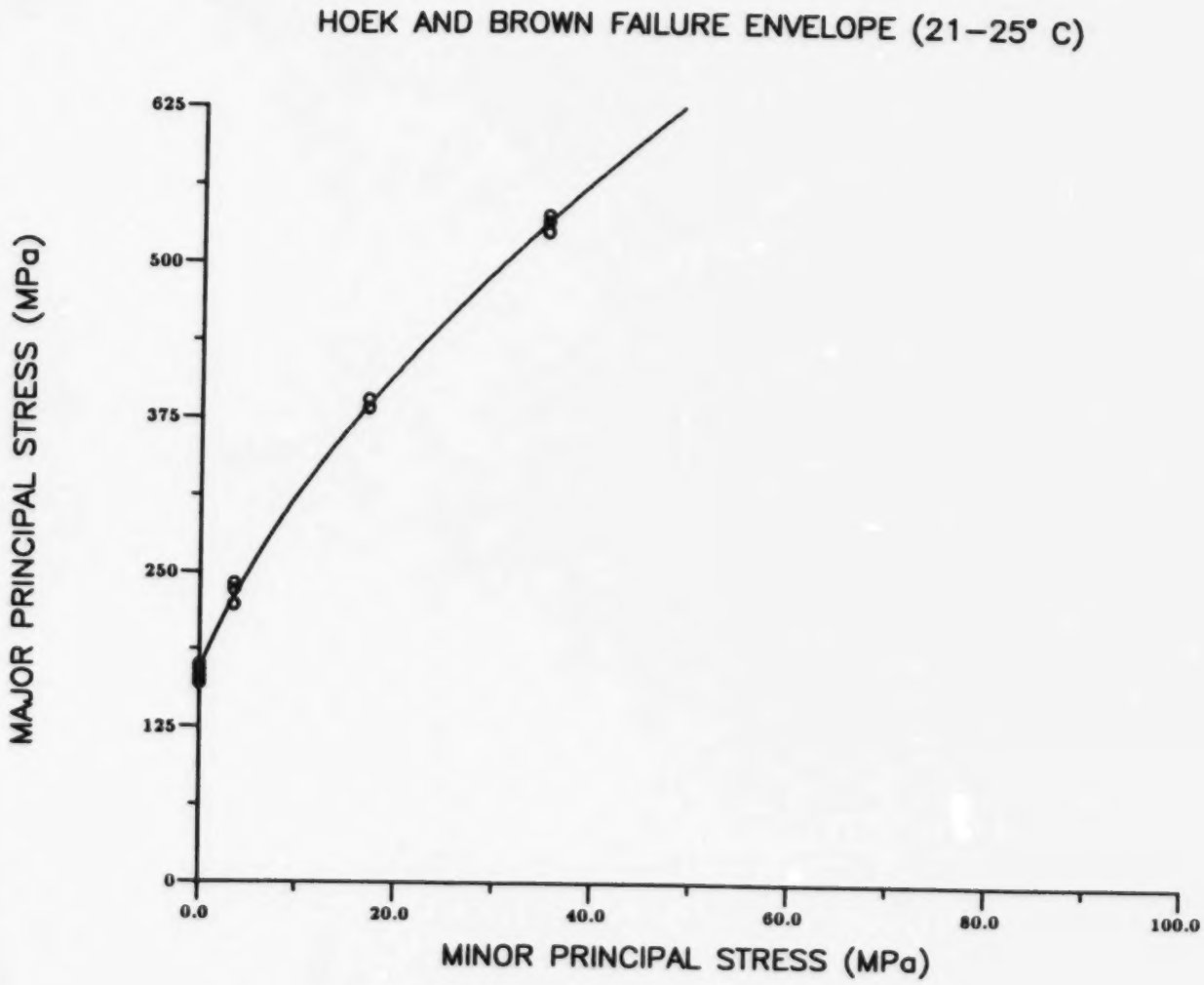

Figure 6. Hoek and Brown failure envelope for tests conducted at 21° – 25° C.

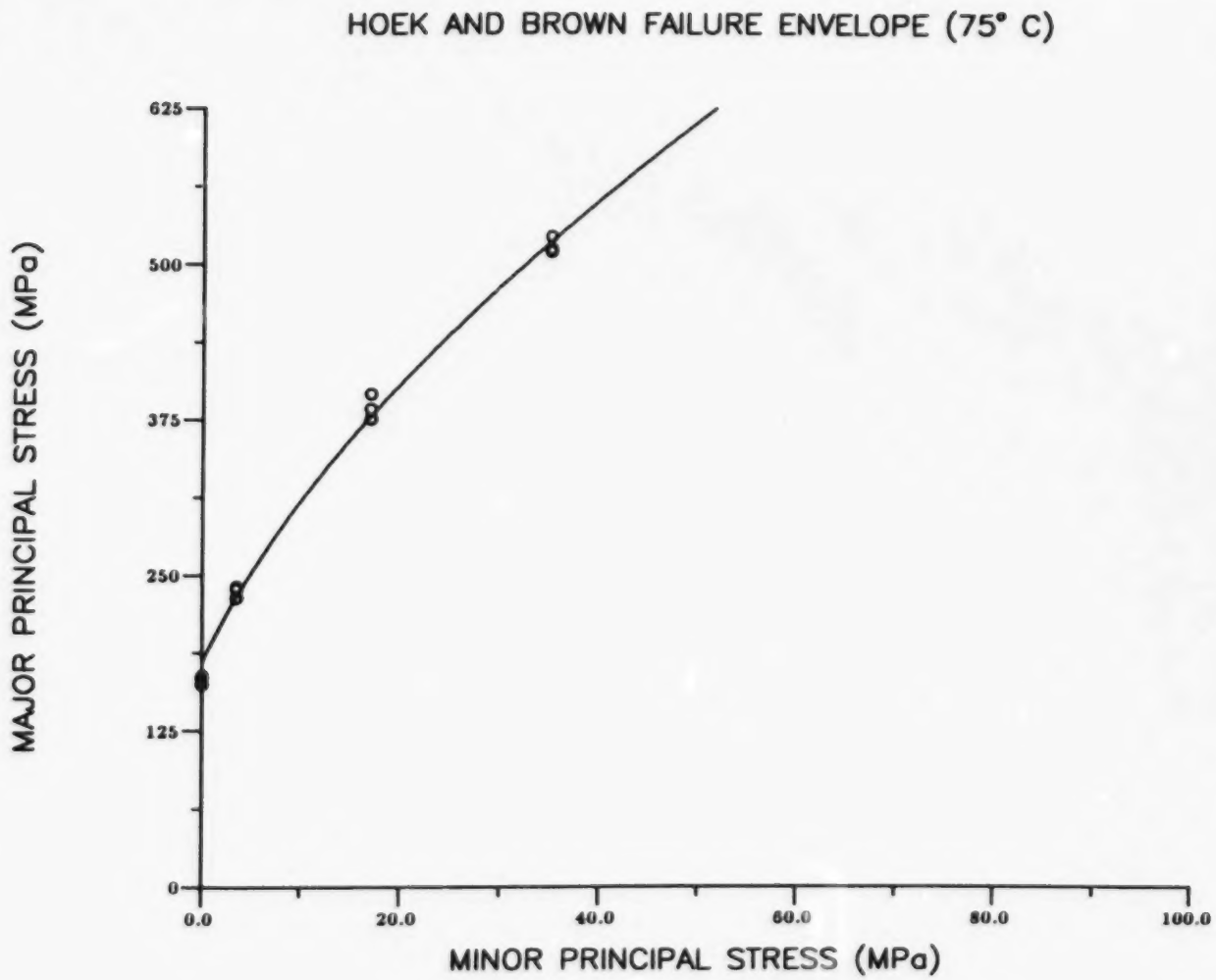

Figure 7. Hoek and Brown failure envelope for tests conducted at 75° C.

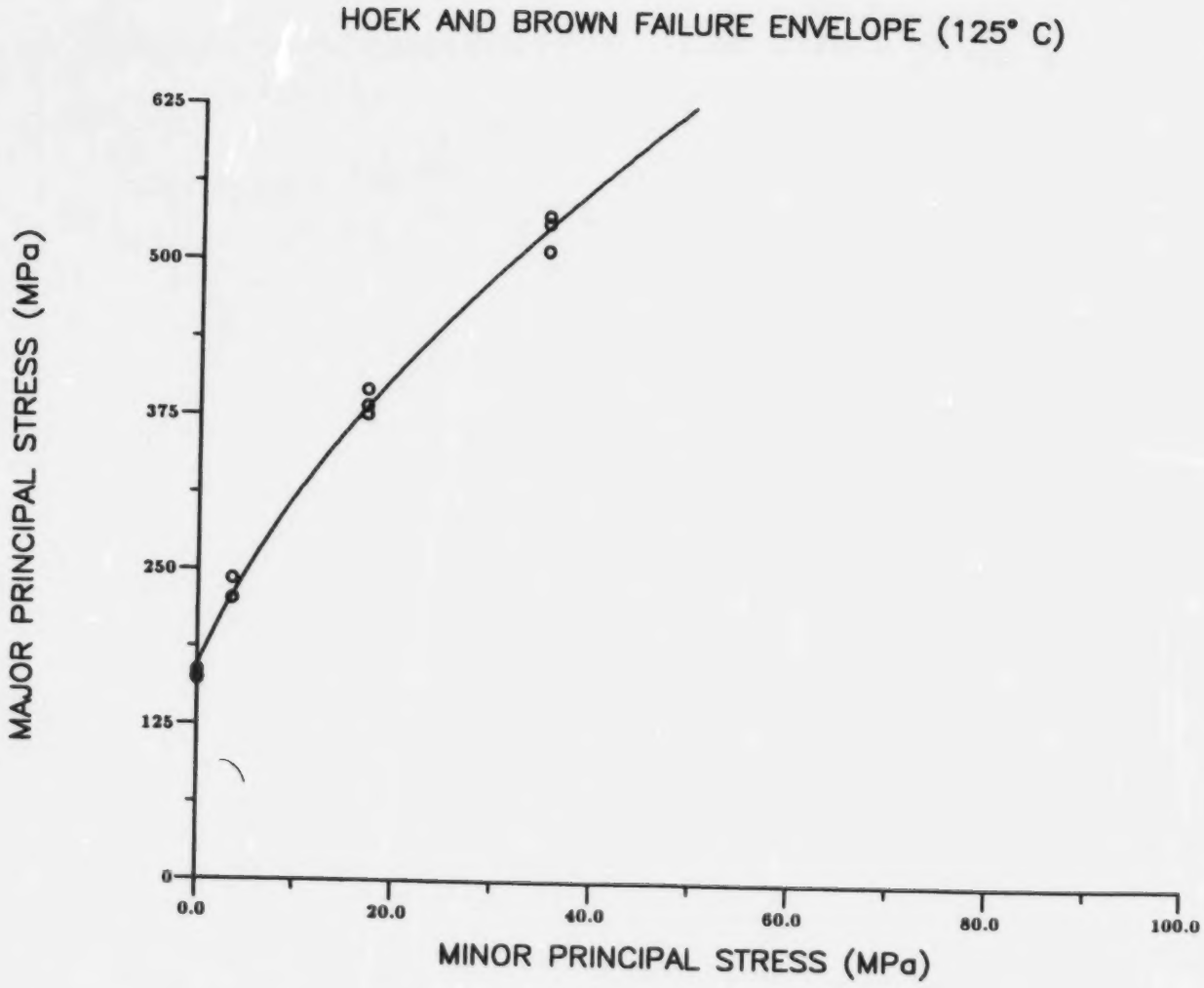

Figure 8. Hoek and Brown failure envelope for tests conducted at 125° C.

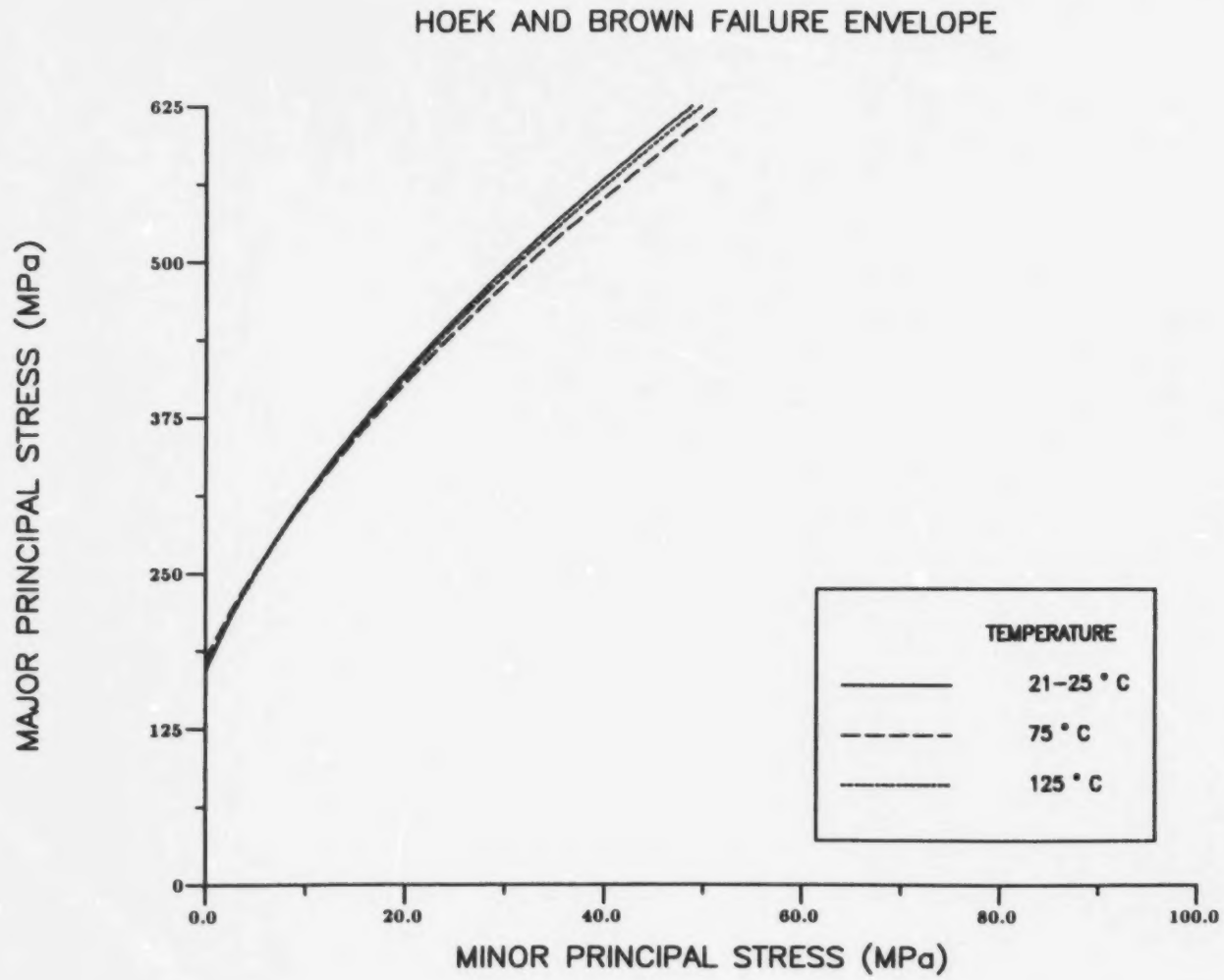

Figure 9. Effect of temperature on the Hoek and Brown failure envelope.

APPENDIX A

Stress-strain Curves for Specimens from
Boreholes 209-018-EXT4 and 209-030-DIL1

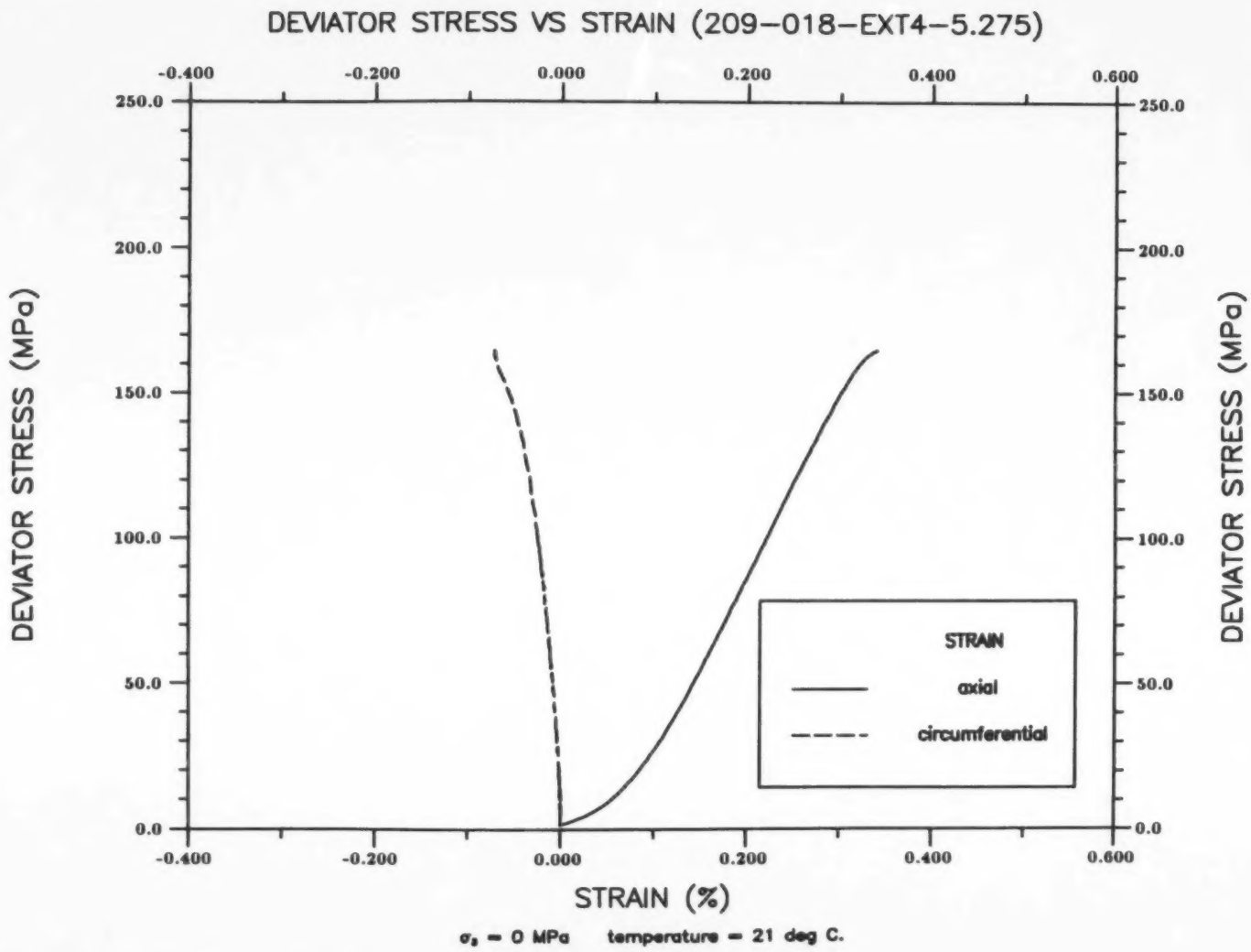

Figure A1. Stress-strain curves for Specimen 209-018-EXT4-5.275 tested at 21° C under the unconfined condition.

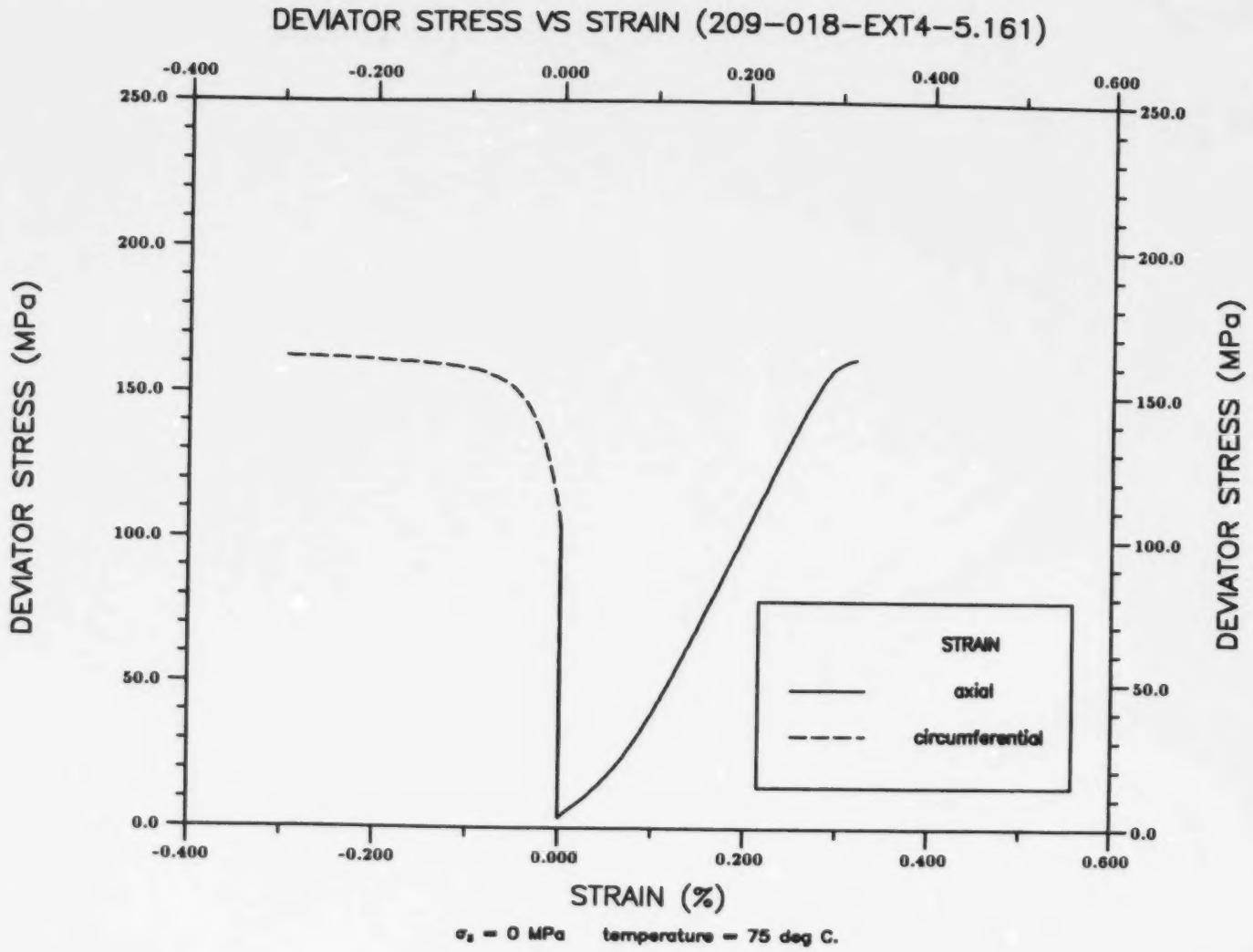

Figure A2. Stress-strain curves for Specimen 209-018-EXT4-5.161 tested at 75° C under the unconfined condition.

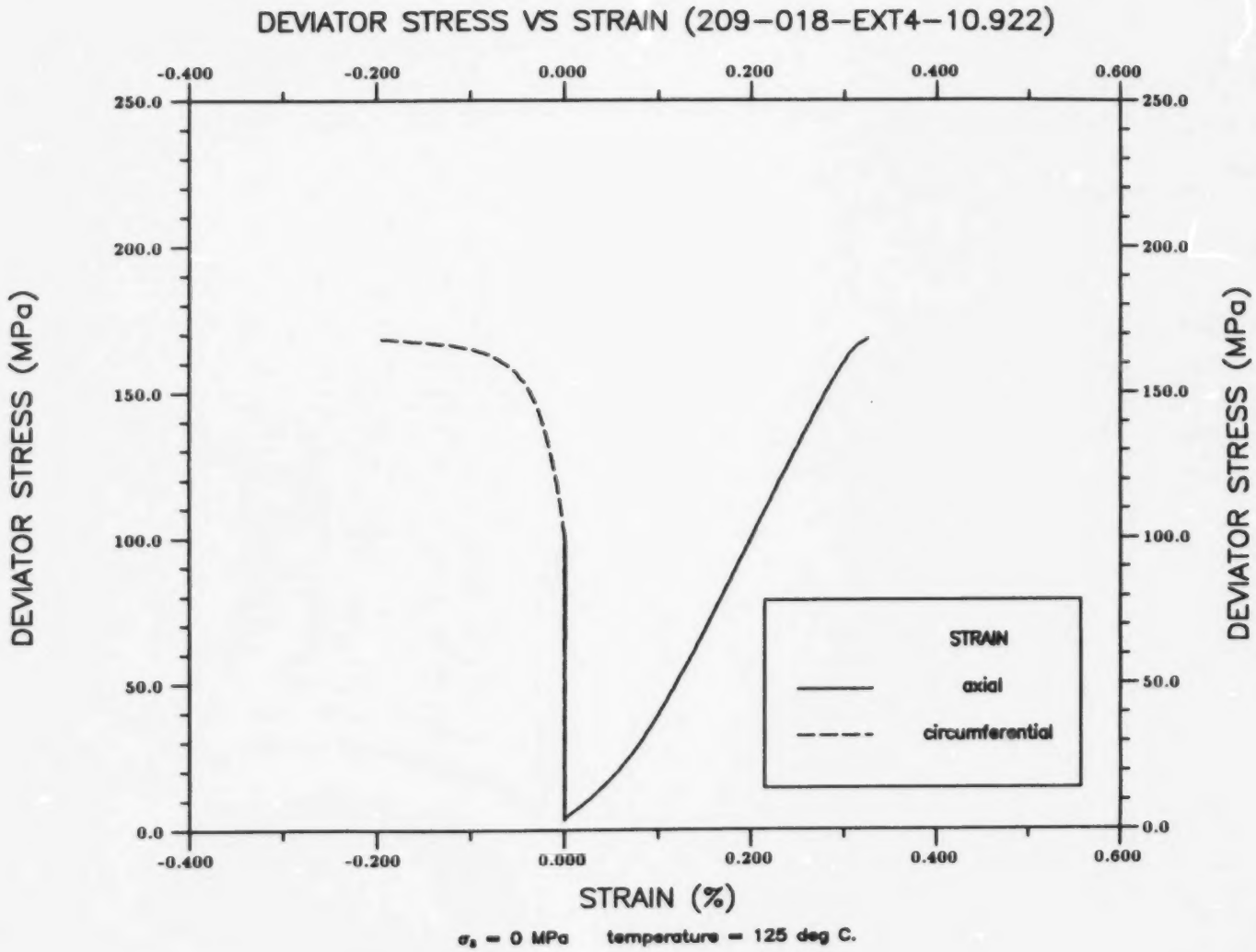

Figure A3. Stress-strain curves for Specimen 209-018-EXT4-10.922 tested at 125° C under the unconfined condition.

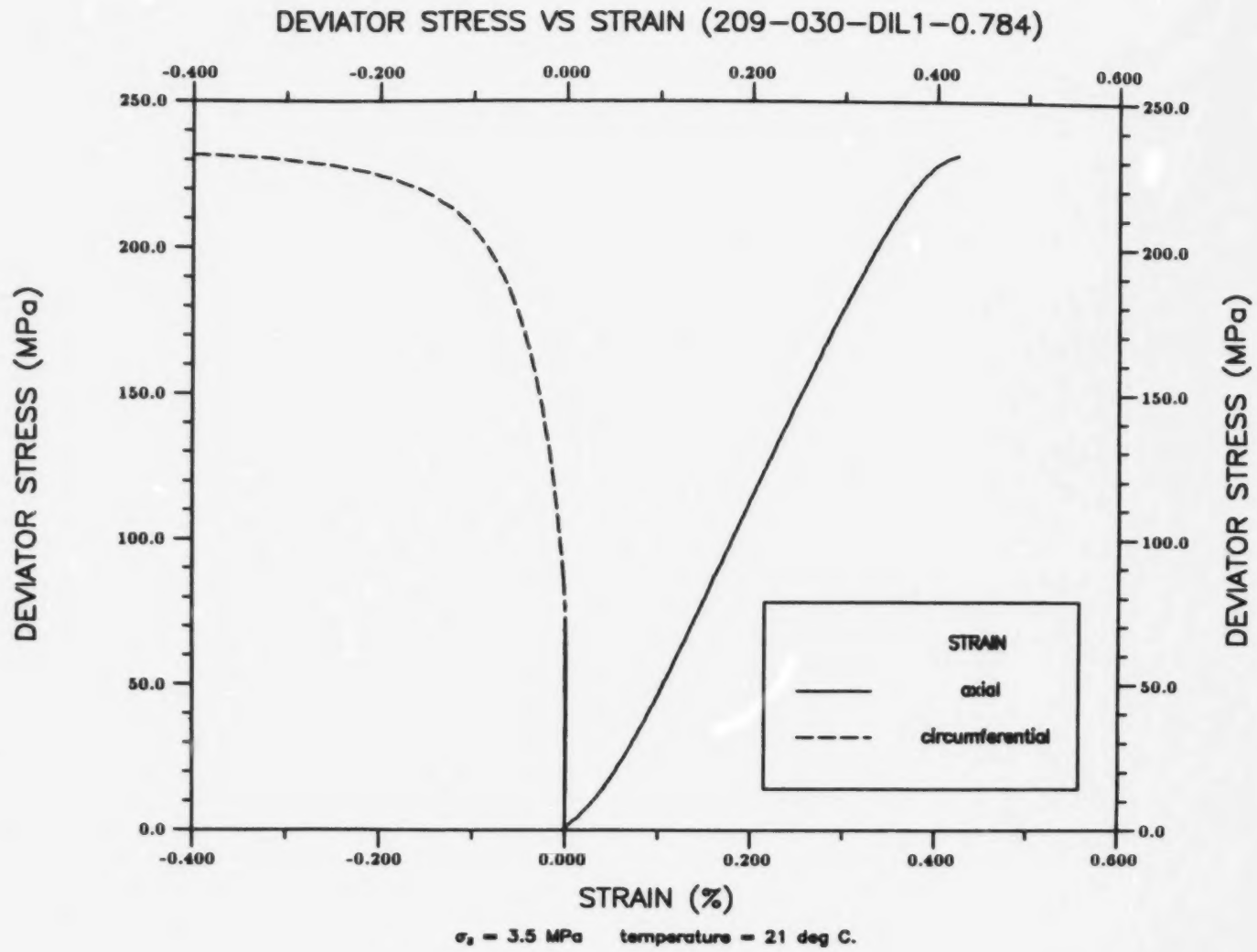

Figure A4. Stress-strain curves for Specimen 209-030-DIL1-0.784 tested at 21° C and at $\sigma_3 = 3.5$ MPa.

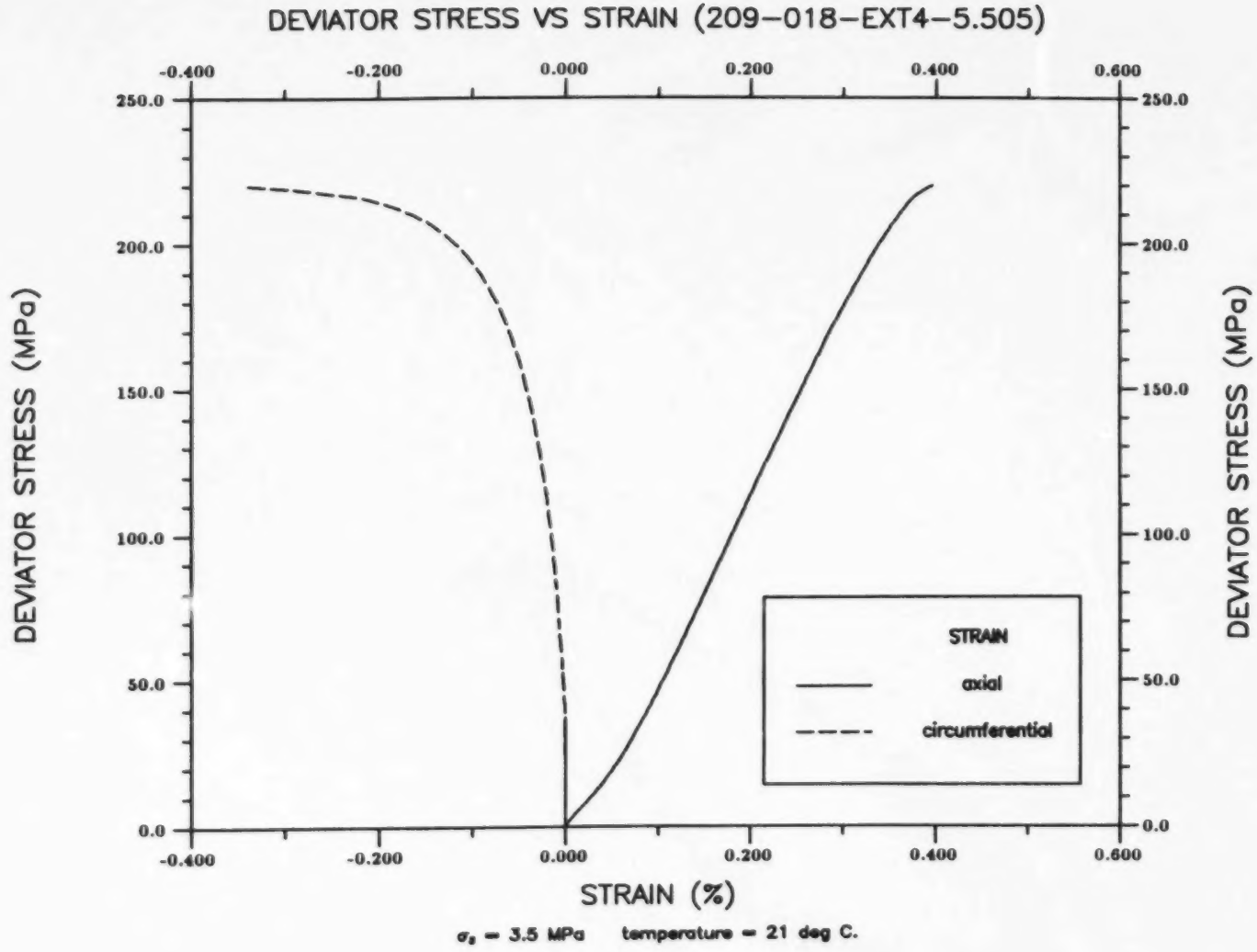

Figure A5. Stress-strain curves for Specimen 209-018-EXT4-5.505 tested at 21° C and at $\sigma_3 = 3.5$ MPa.

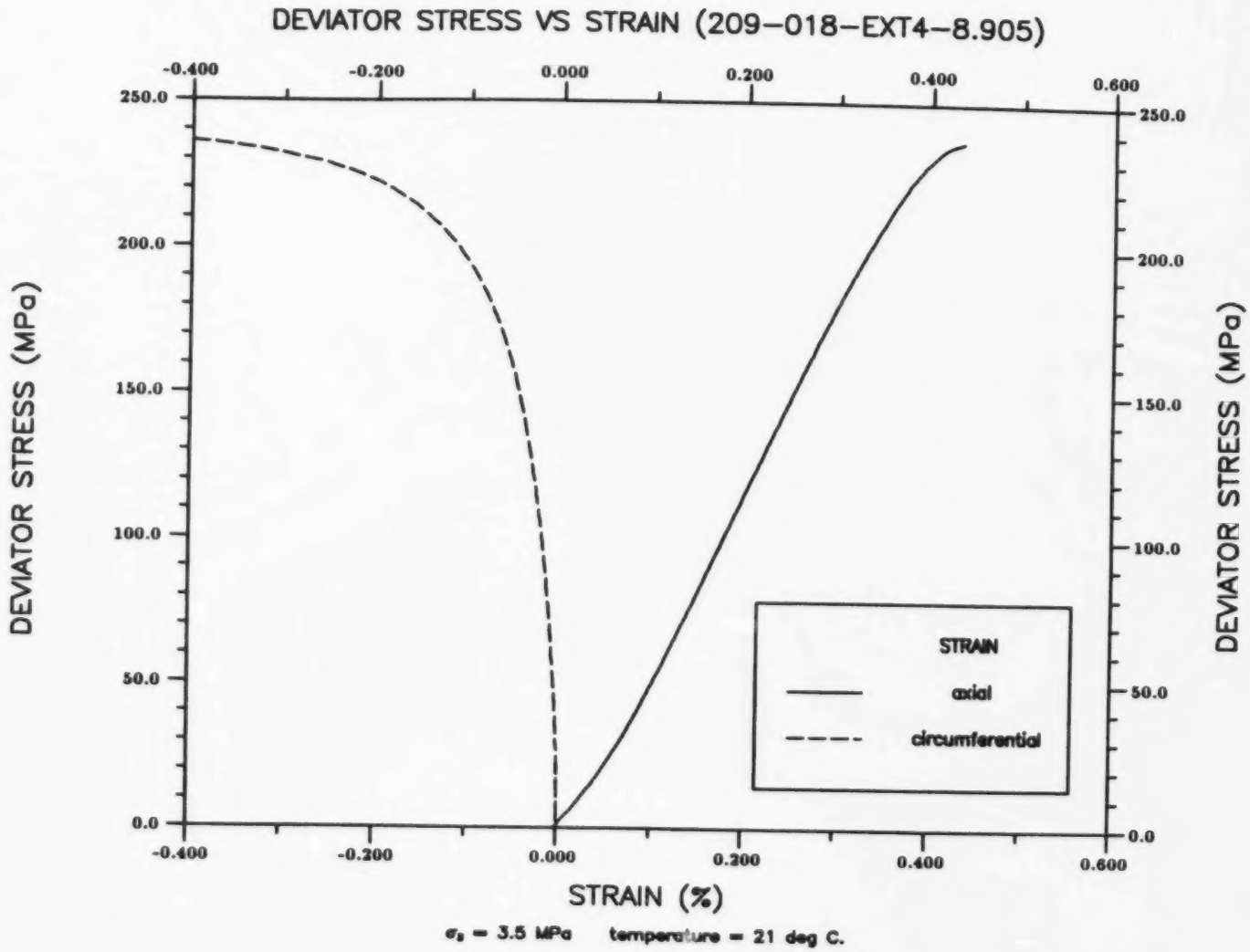

Figure A6. Stress-strain curves for Specimen 209-018-EXT4-8.905 tested at 21° C and at $\sigma_3 = 3.5$ MPa.

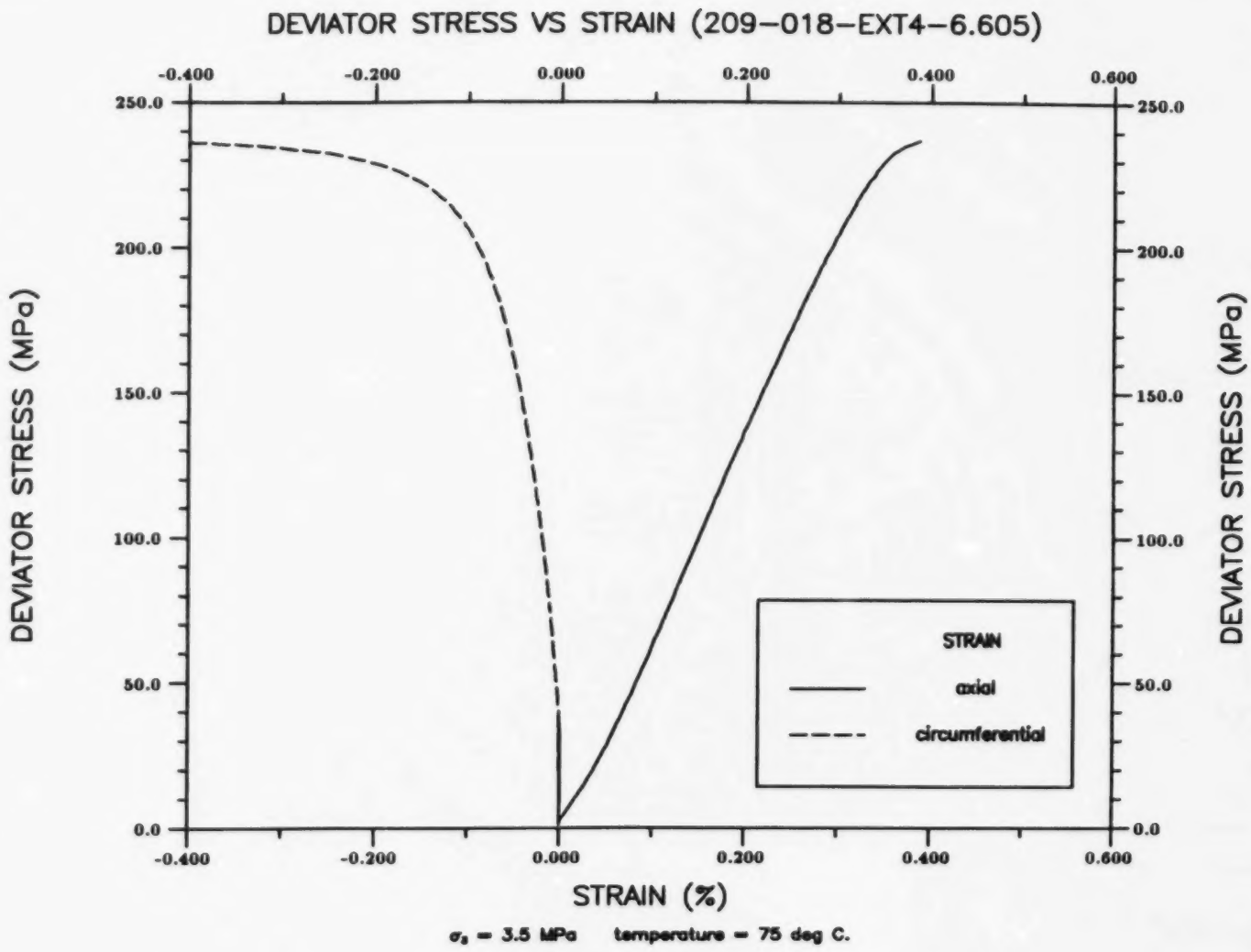

Figure A7. Stress-strain curves for Specimen 209-018-EXT4-6.605 tested at 75° C and at $\sigma_3 = 3.5$ MPa.

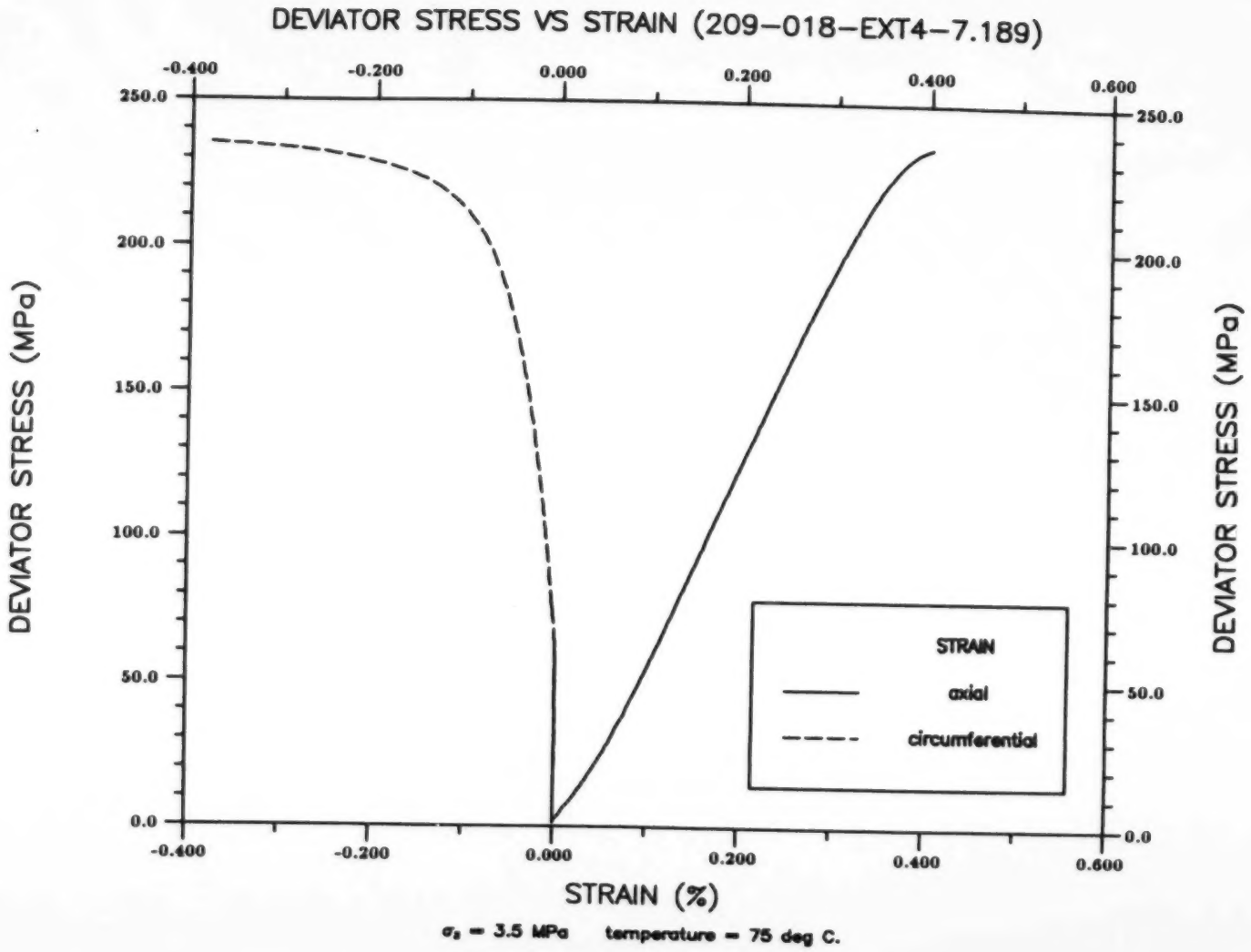

Figure A8. Stress-strain curves for Specimen 209-018-EXT4-7.189 tested at 75° C and at $\sigma_3 = 3.5$ MPa.

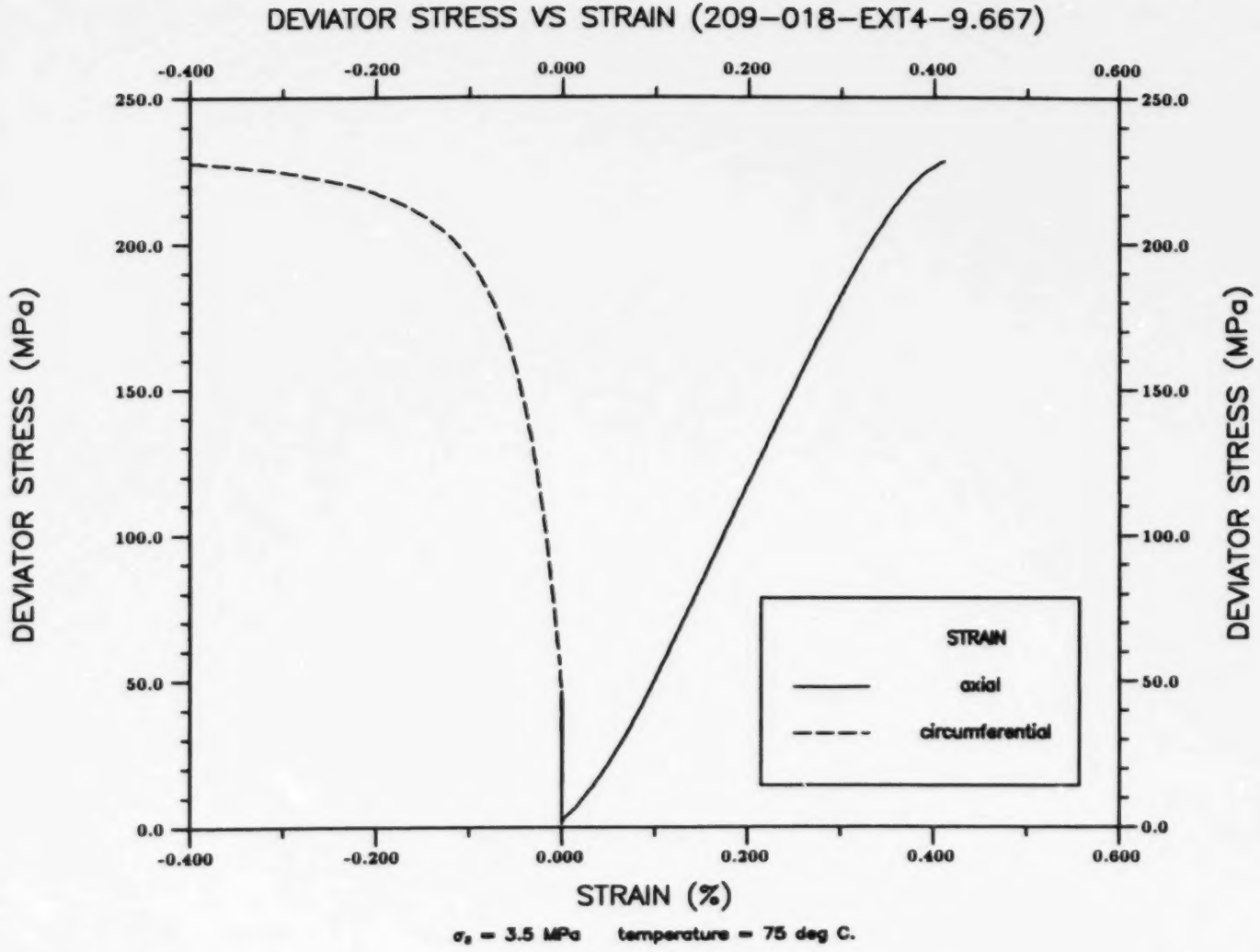

Figure A9. Stress-strain curves for Specimen 209-018-EXT4-9.667 tested at 75° C and at $\sigma_3 = 3.5$ MPa.

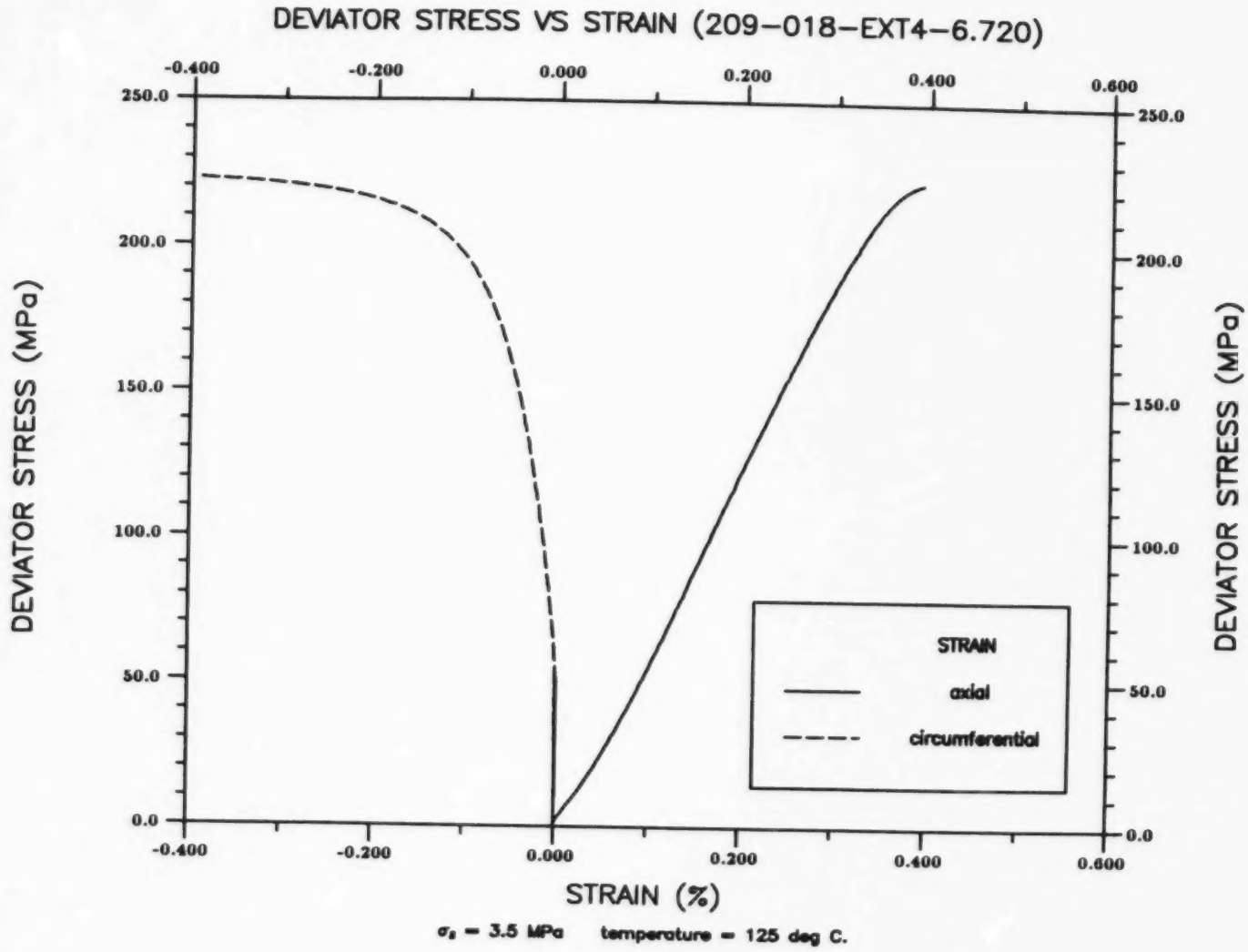

Figure A10. Stress-strain curves for Specimen 209-018-EXT4-6.720 tested at 125° C and at $\sigma_3 = 3.5$ MPa.

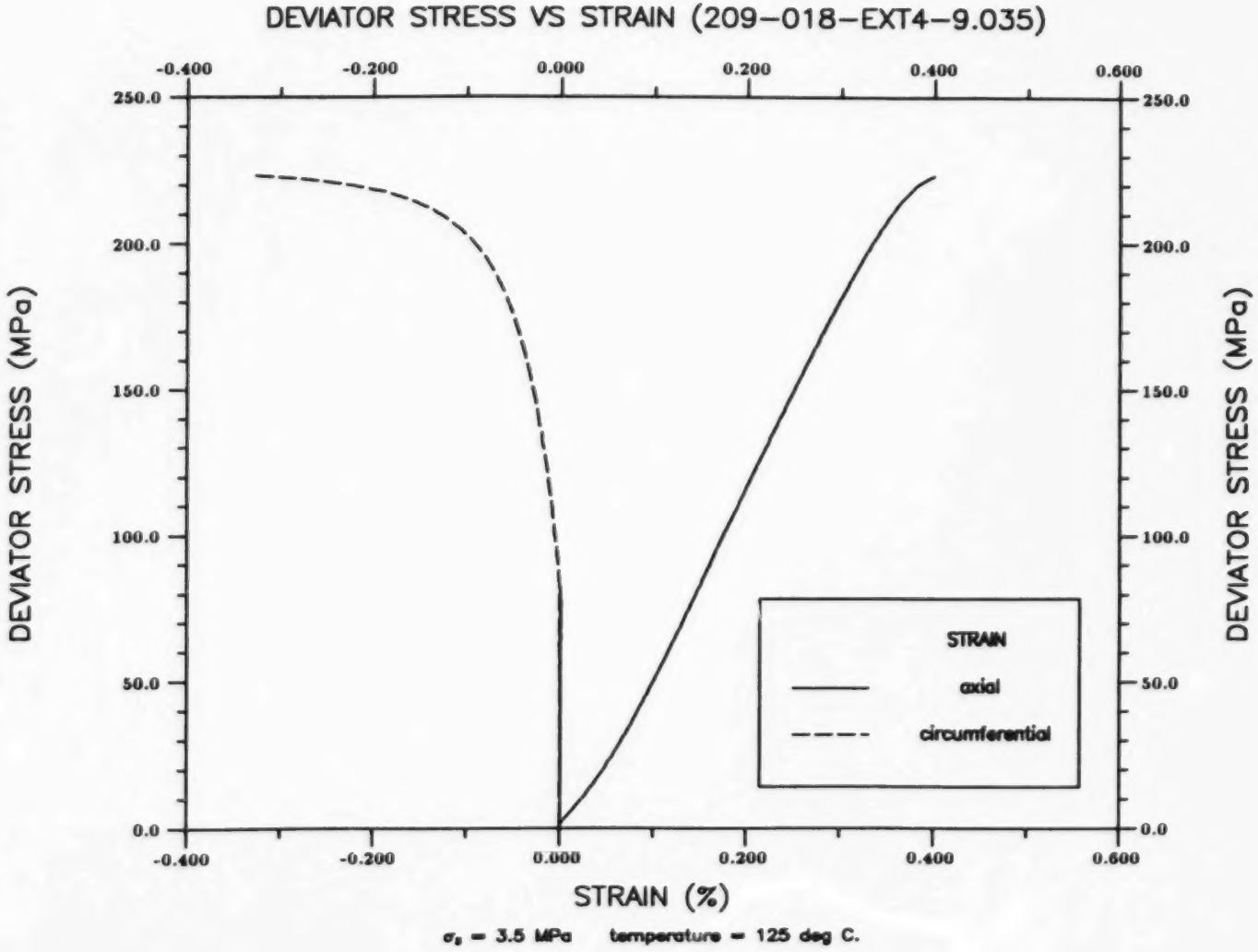

Figure A11. Stress-strain curves for Specimen 209-018-EXT4-9.035 tested at 125° C and at $\sigma_3 = 3.5$ MPa.

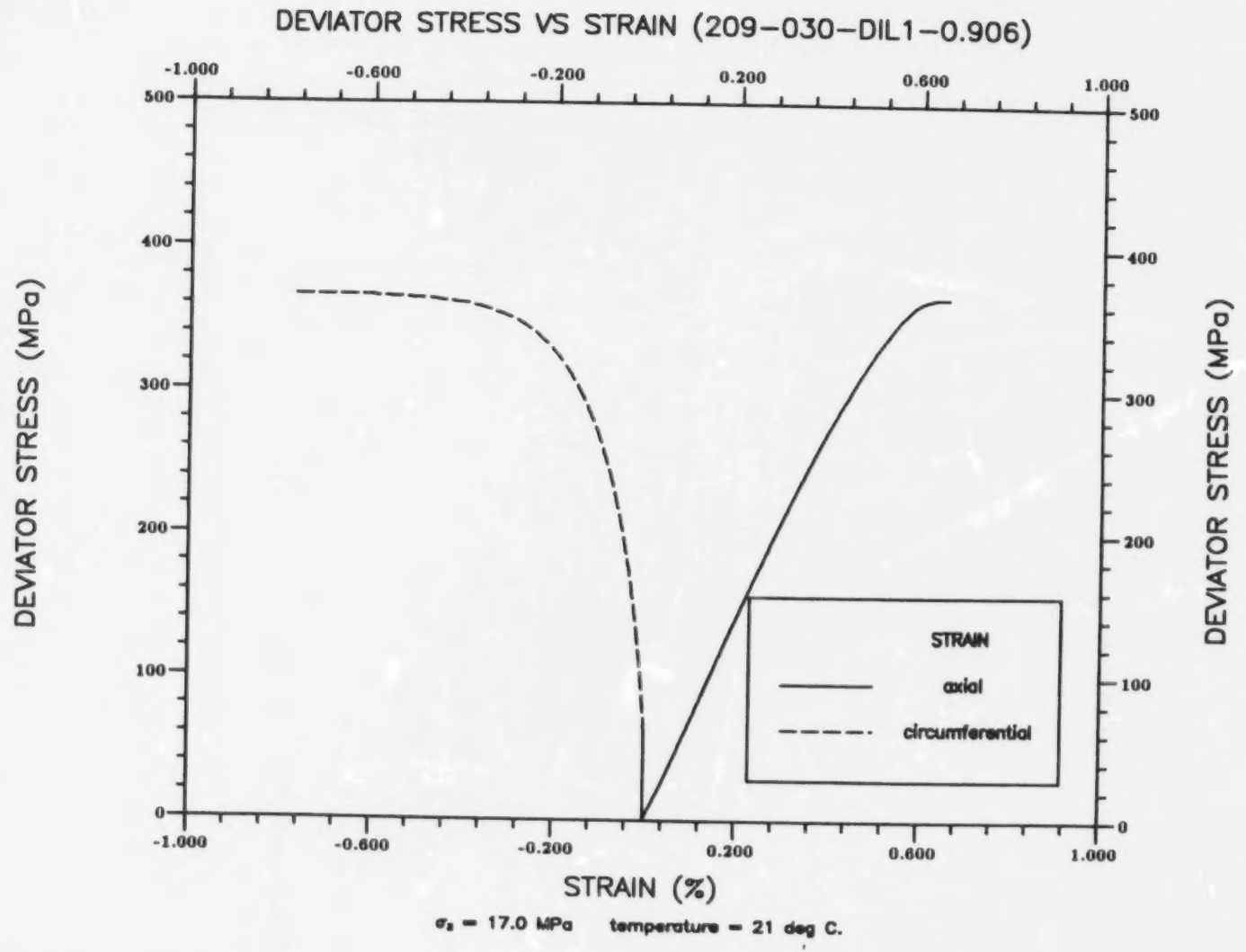

Figure A12. Stress-strain curves for Specimen 209-030-DIL1-0.906 tested at 21° C and at $\sigma_3 = 17$ MPa.

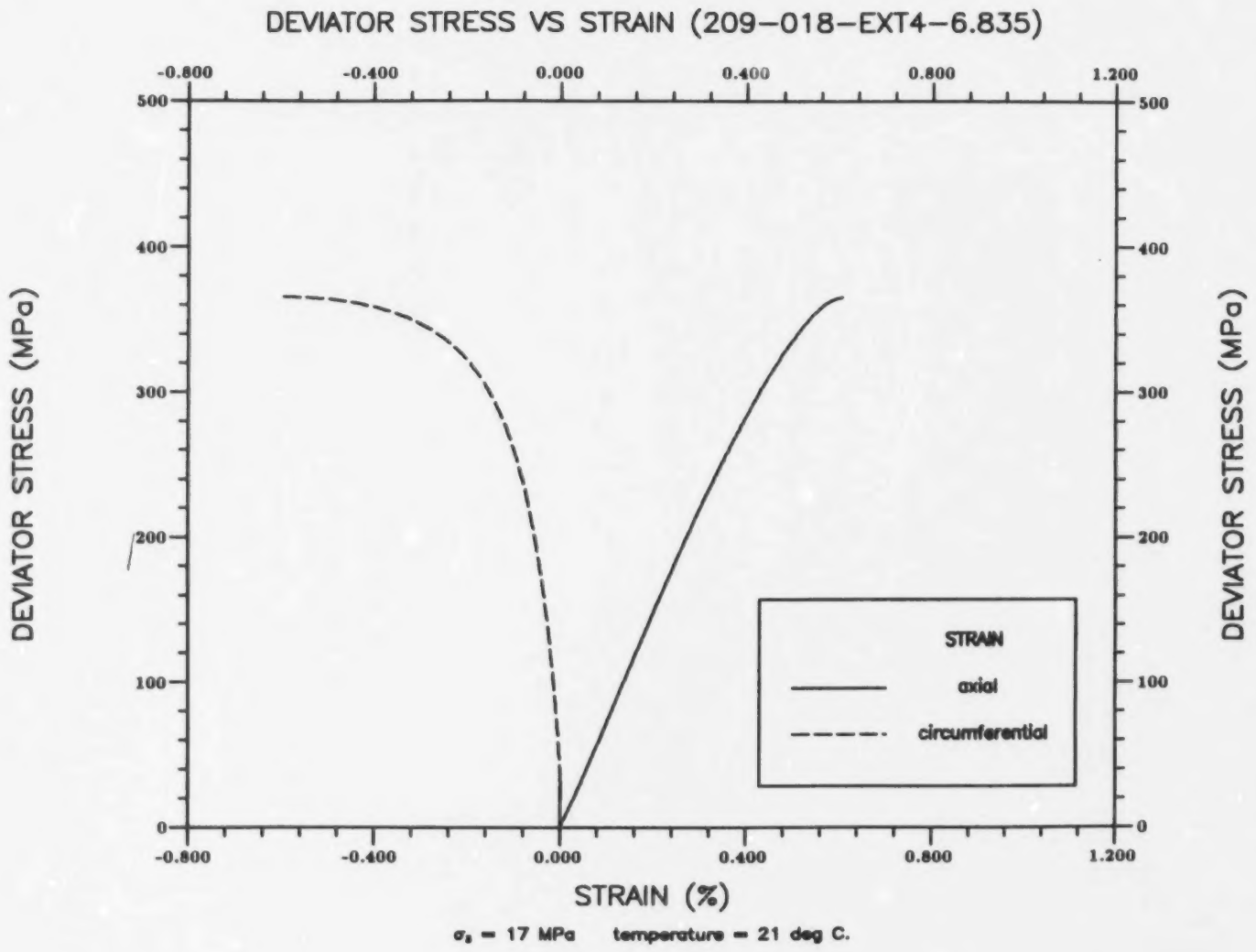

Figure A13. Stress-strain curves for Specimen 209-018-EXT4-6.835 tested at 21° C and at $\sigma_3 = 17$ MPa.

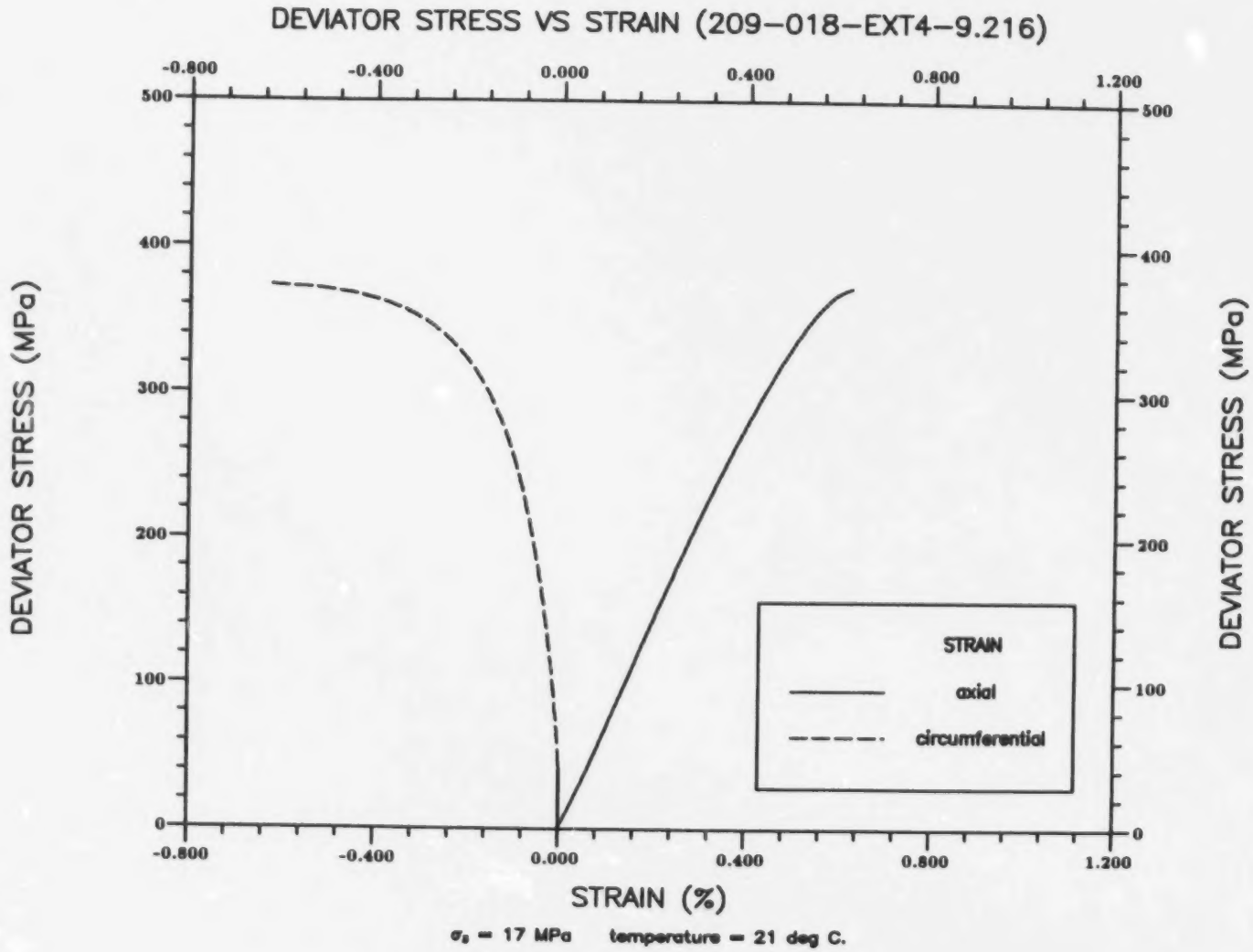

Figure A14. Stress-strain curves for Specimen 209-018-EXT4-9.216 tested at 21° C and at $\sigma_3 = 17$ MPa.

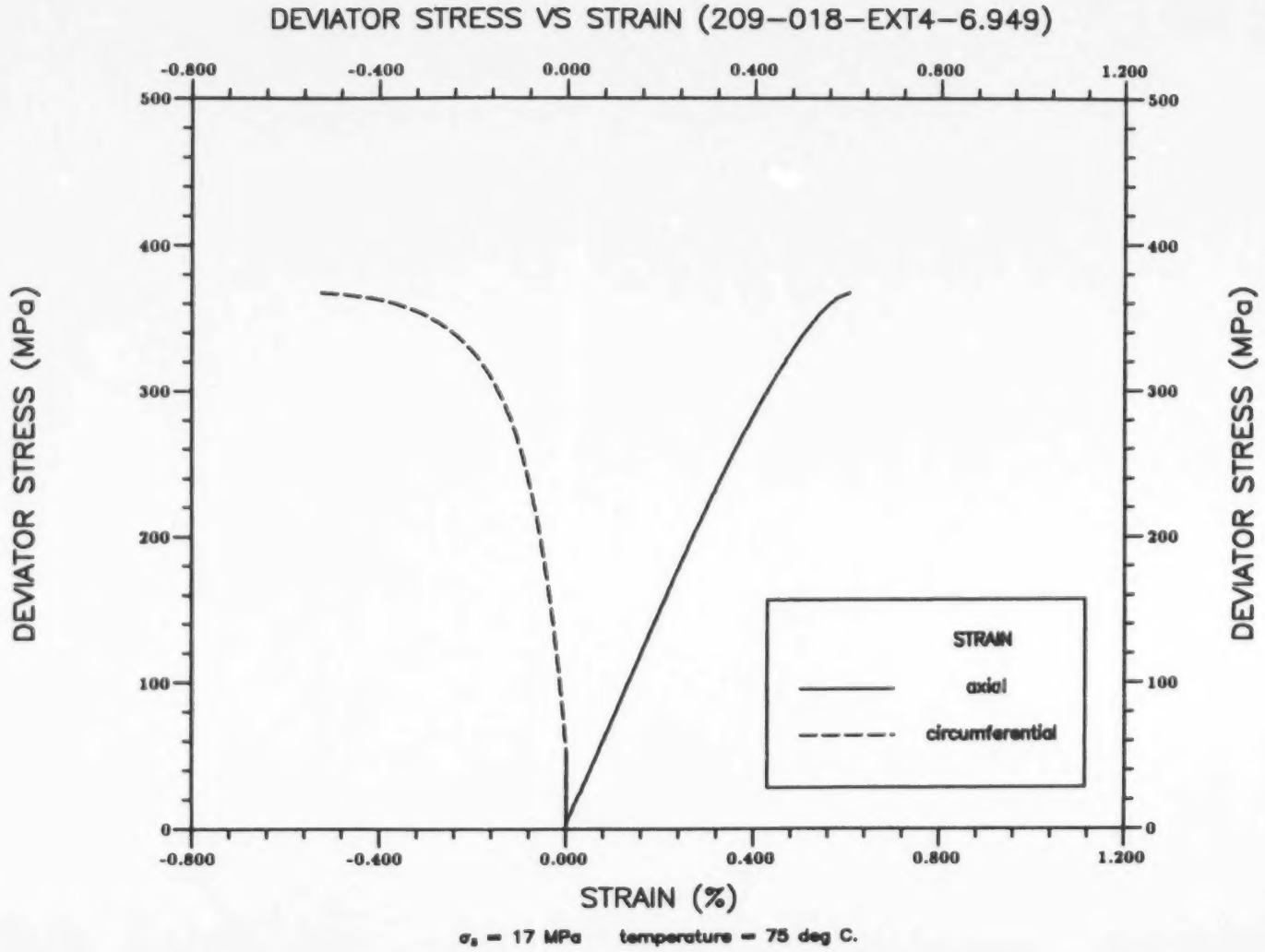

Figure A15. Stress-strain curves for Specimen 209-018-EXT4-6.949 tested at 75° C and at $\sigma_3 = 17$ MPa.

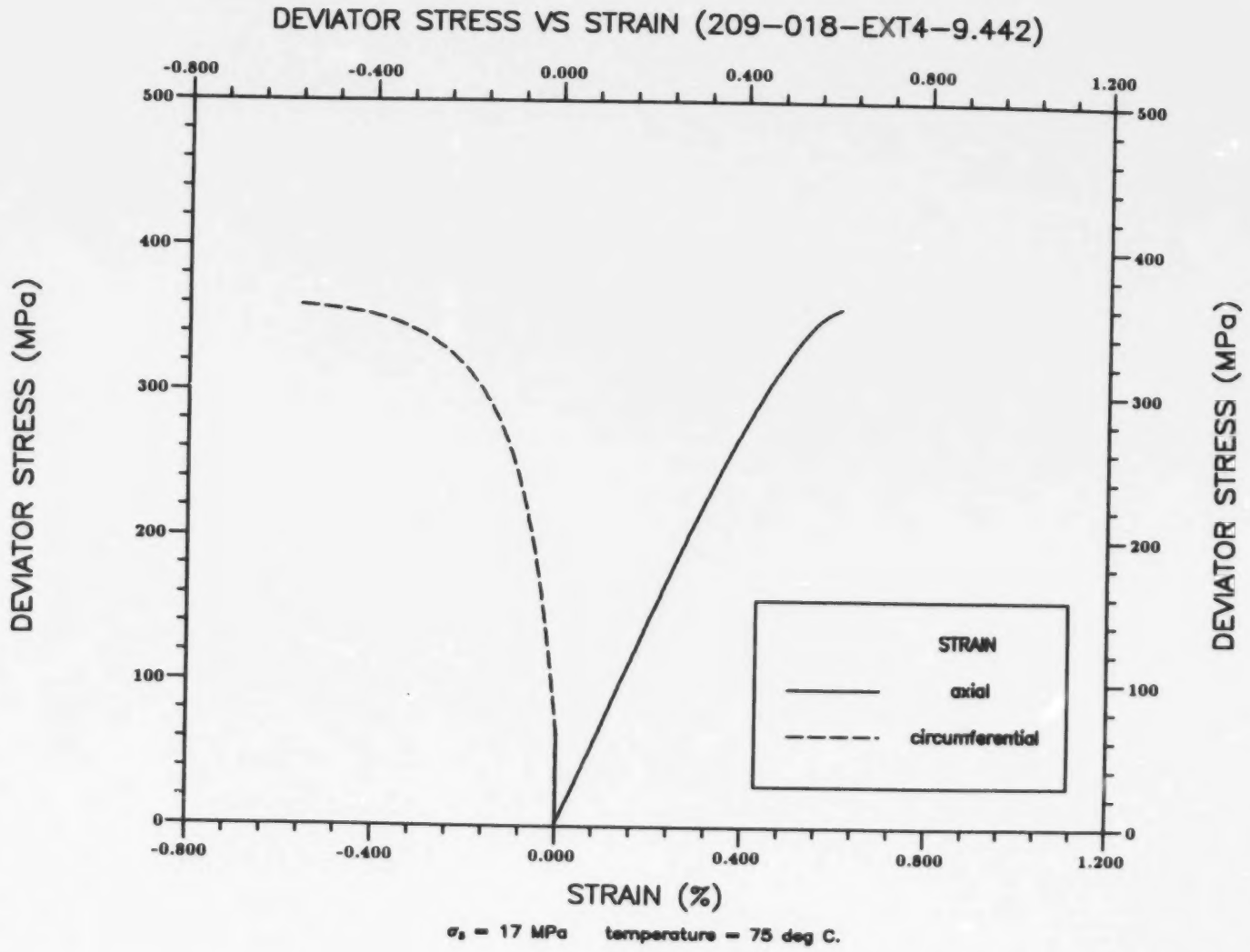

Figure A16. Stress-strain curves for Specimen 209-018-EXT4-9.442 tested at 75° C and at $\sigma_3 = 17$ MPa.

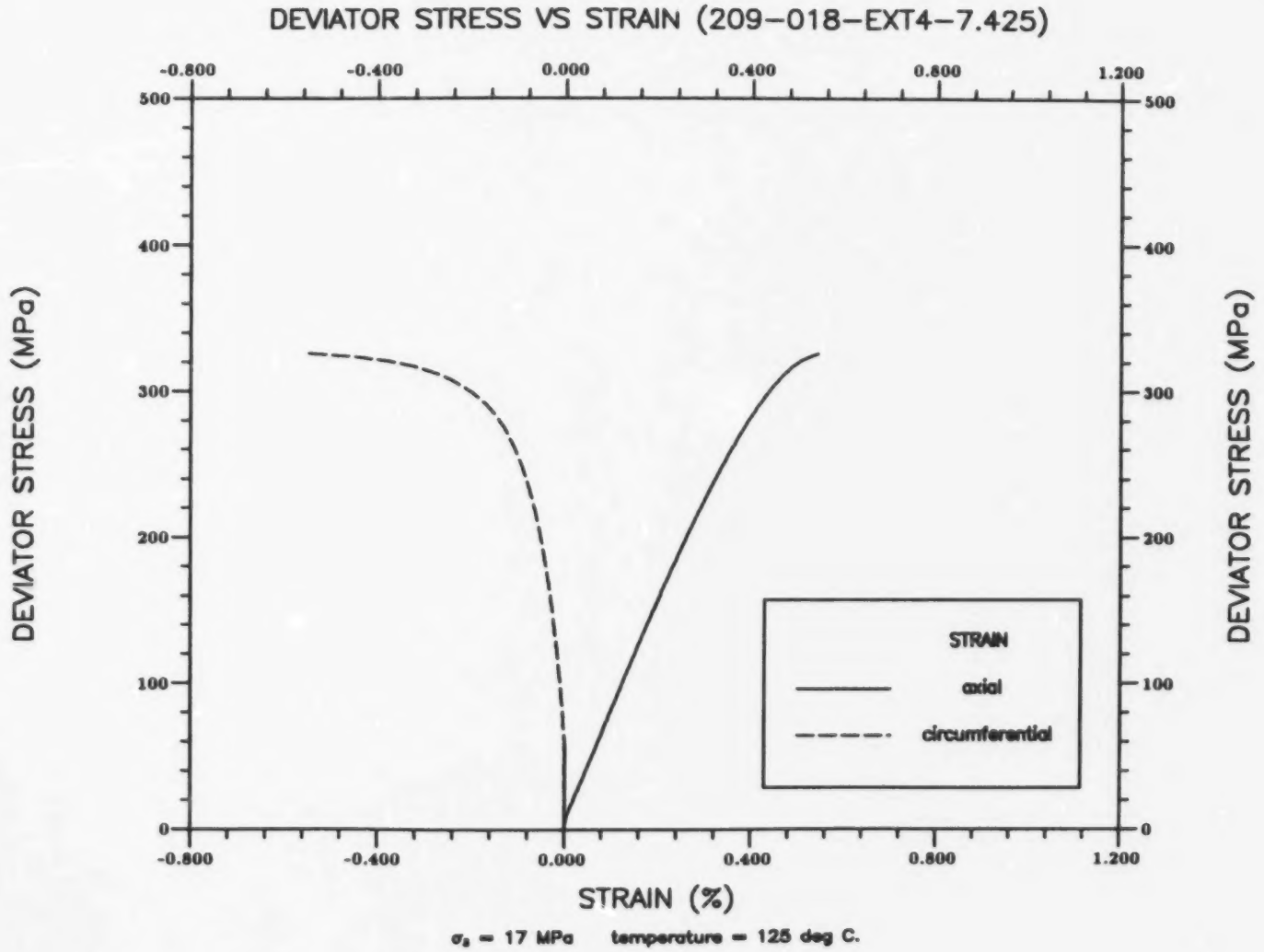

Figure A17. Stress-strain curves for Specimen 209-018-EXT4-7.425 tested at 125° C and at $\sigma_3 = 17$ MPa.

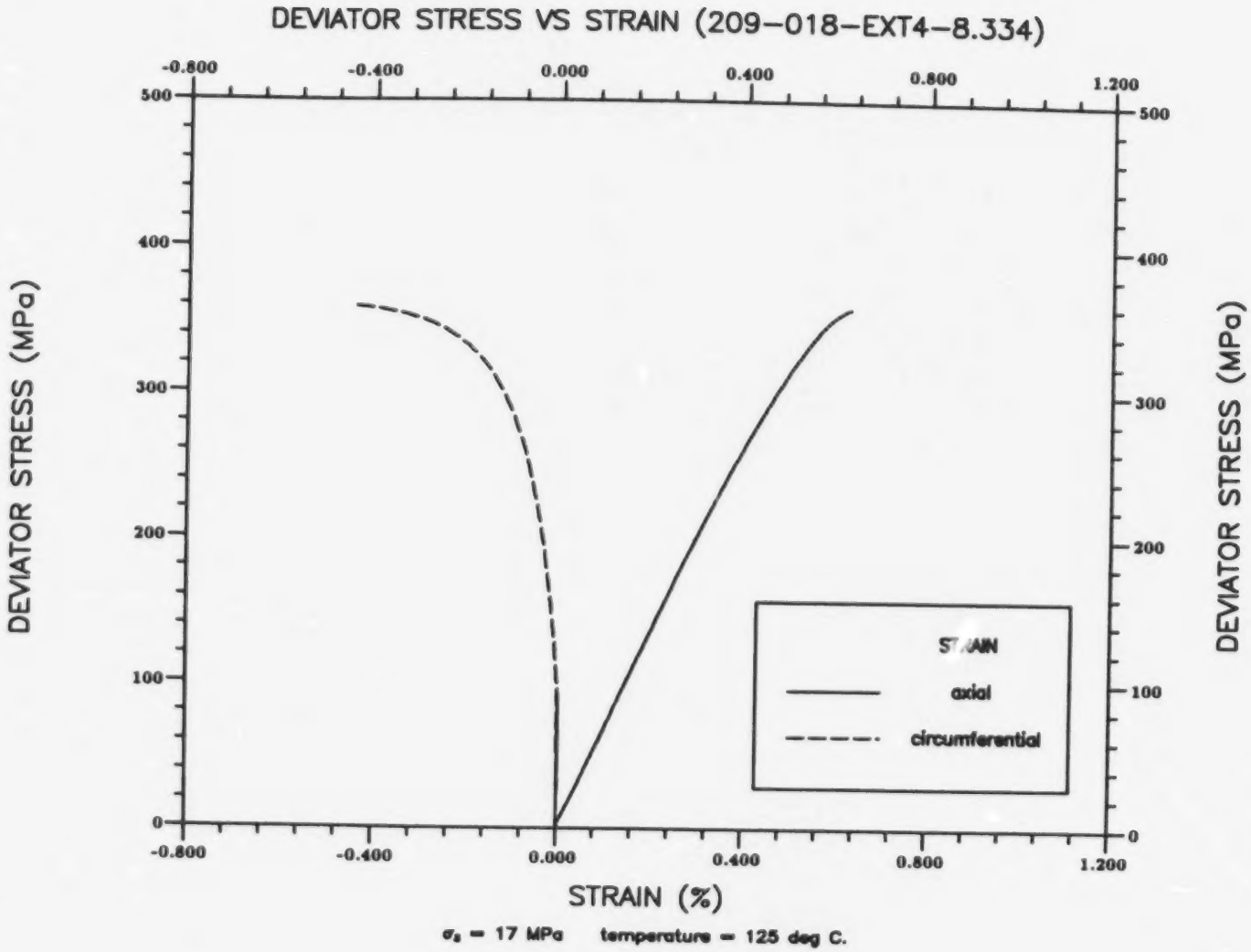

Figure A18. Stress-strain curves for Specimen 209-018-EXT4-8.334 tested at 125° C and at $\sigma_3 = 17$ MPa.

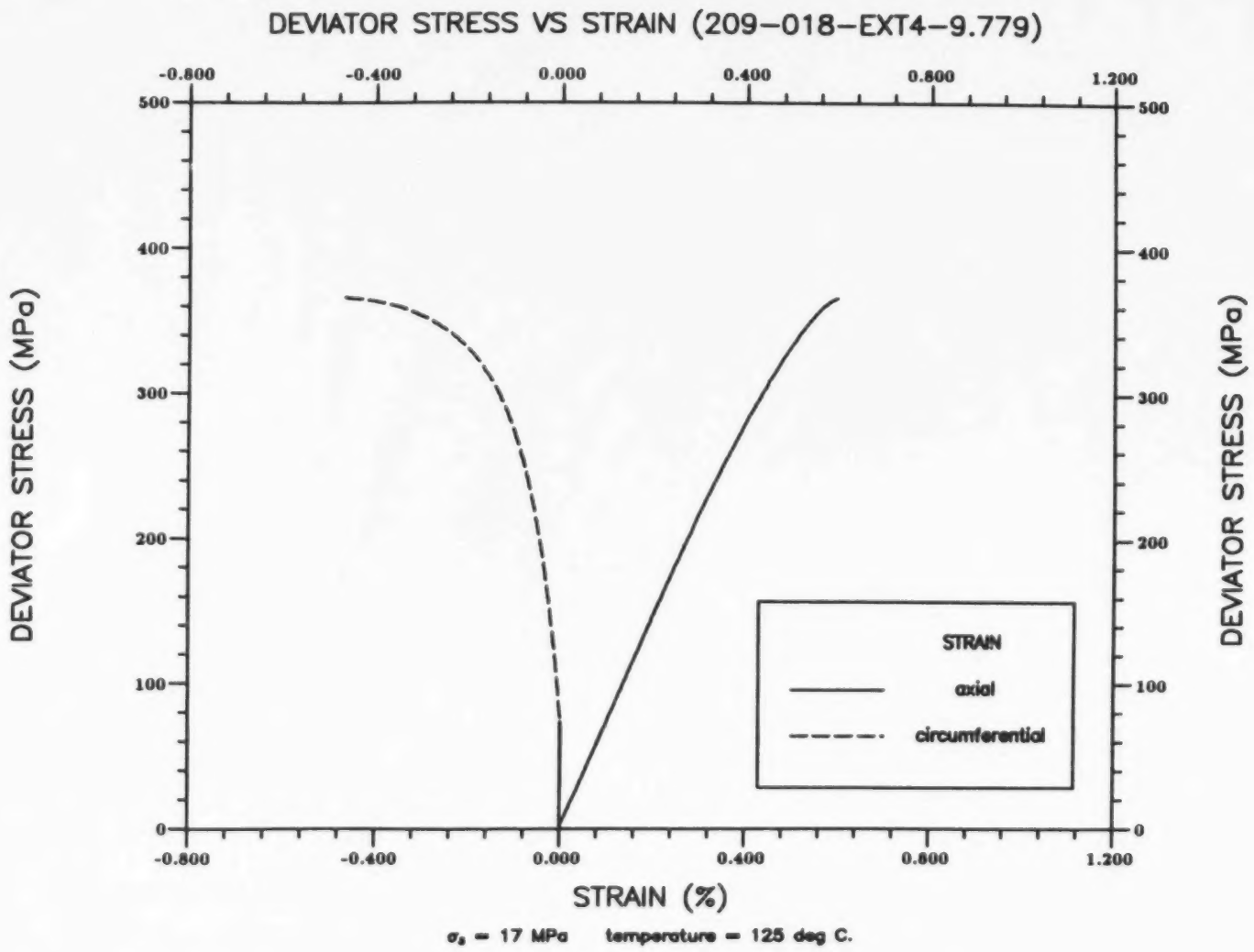

Figure A19. Stress-strain curves for Specimen 209-018-EXT4-9.779 tested at 125° C and at $\sigma_3 = 17$ MPa.

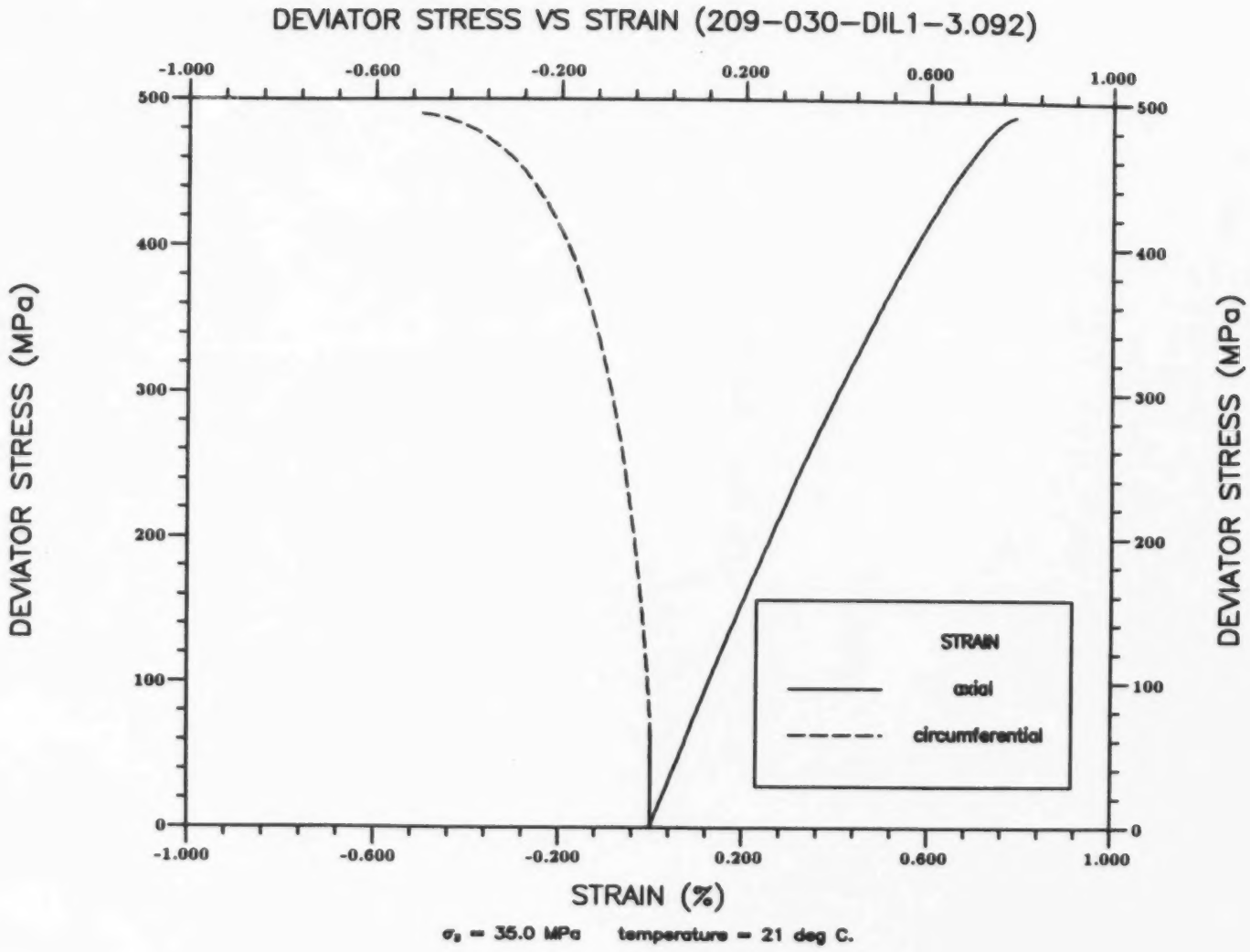

Figure A20. Stress-strain curves for Specimen 209-030-DIL1-3.092 tested at 21° C and at $\sigma_3 = 35$ MPa.

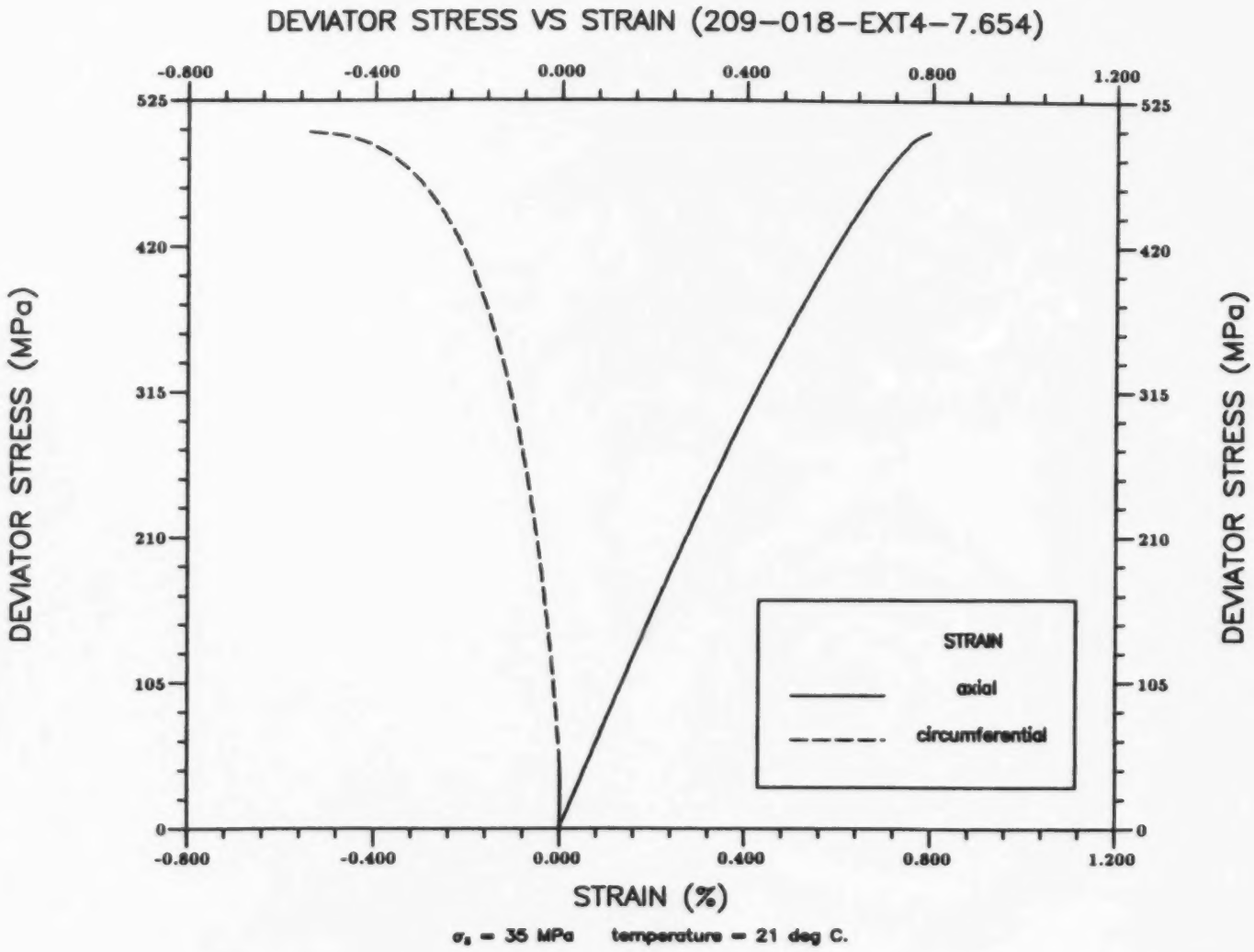

Figure A21. Stress-strain curves for Specimen 209-018-EXT4-7.654 tested at 21° C and at $\sigma_3 = 35$ MPa.

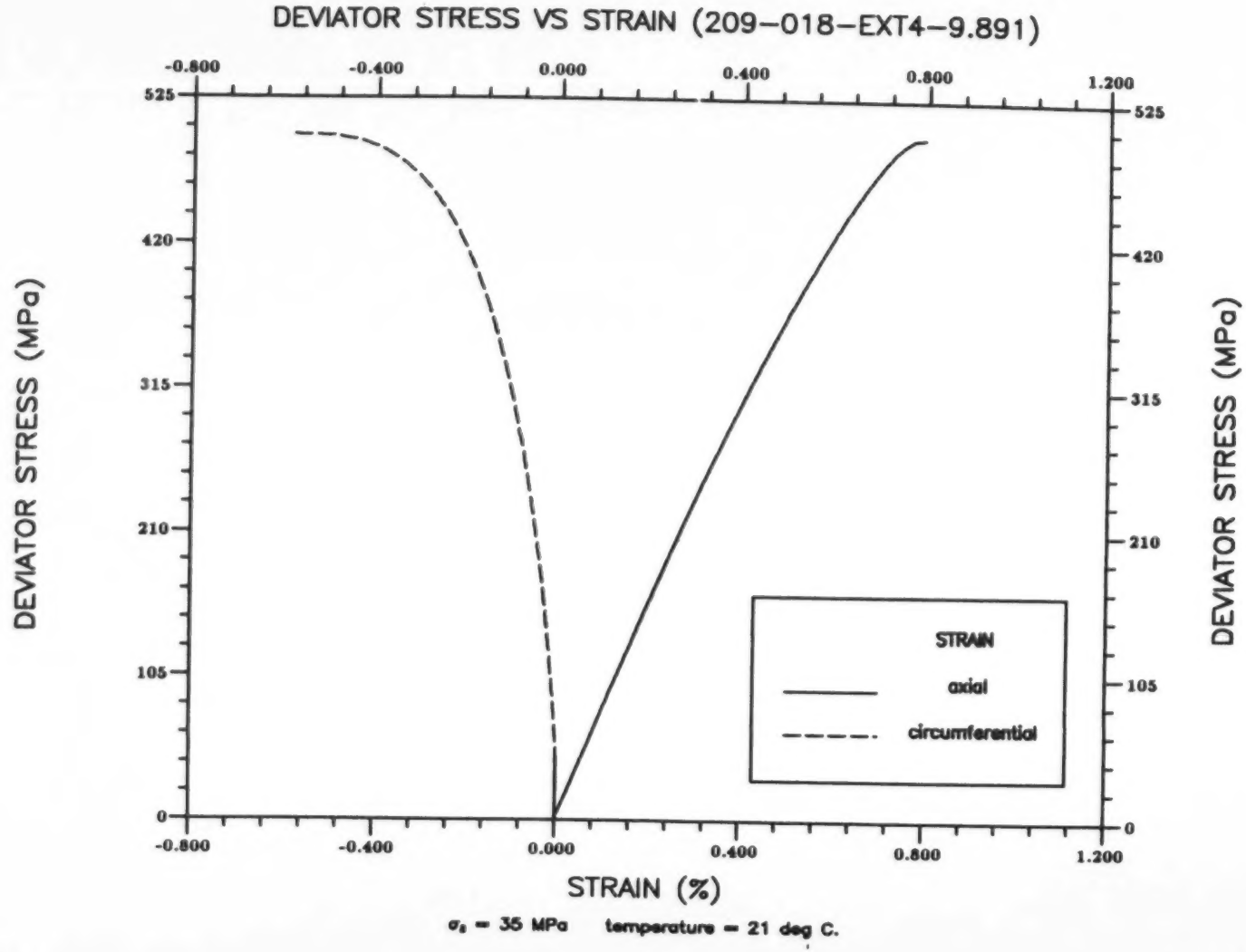

Figure A22. Stress-strain curves for Specimen 209-018-EXT4-9.891 tested at 21° C and at $\sigma_3 = 35$ MPa.

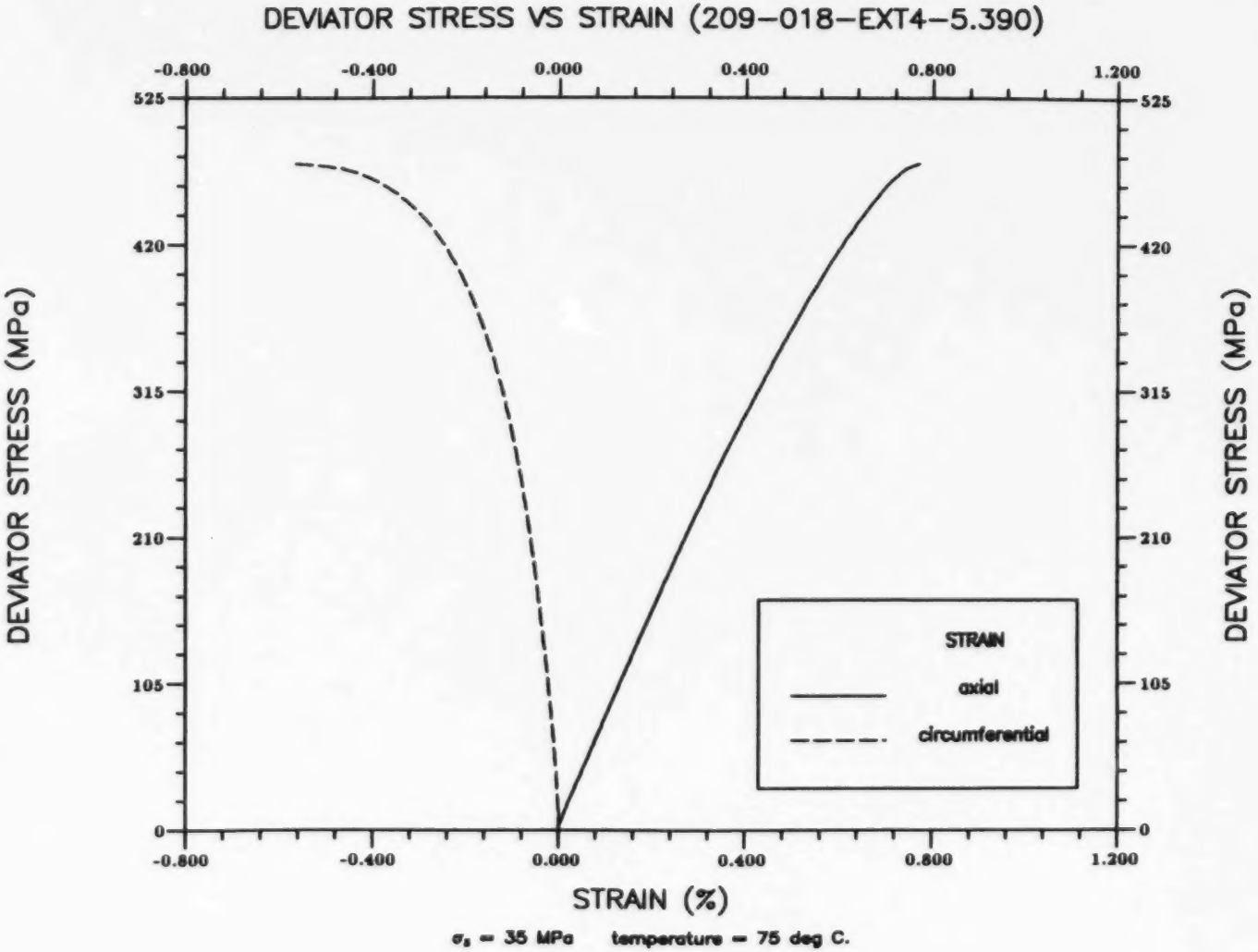

Figure A23. Stress-strain curves for Specimen 209-018-EXT4-5.390 tested at 75° C and at $\sigma_3 = 35$ MPa.

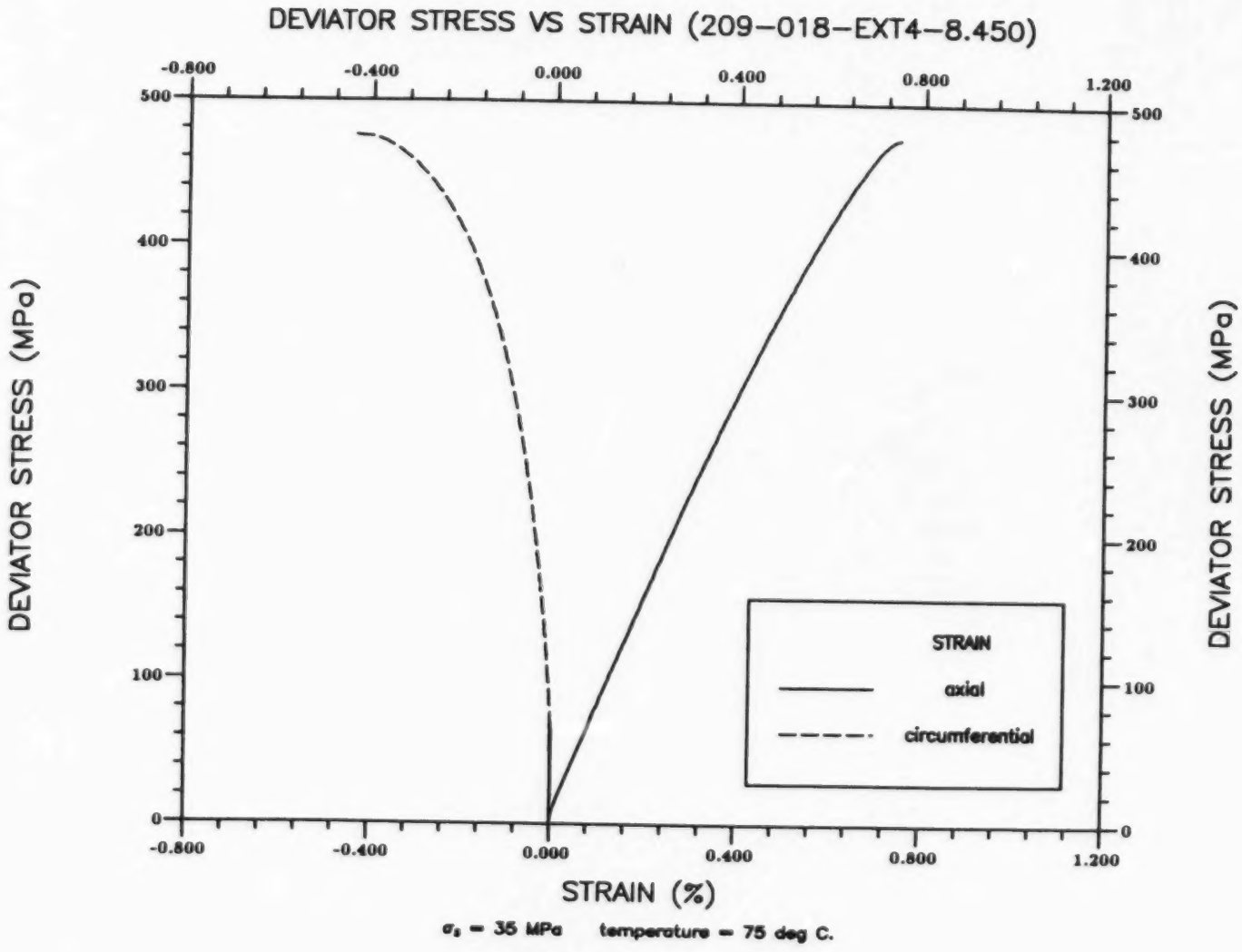

Figure A24. Stress-strain curves for Specimen 209-018-EXT4-8.450 tested at 75° C and at $\sigma_3 = 35$ MPa.

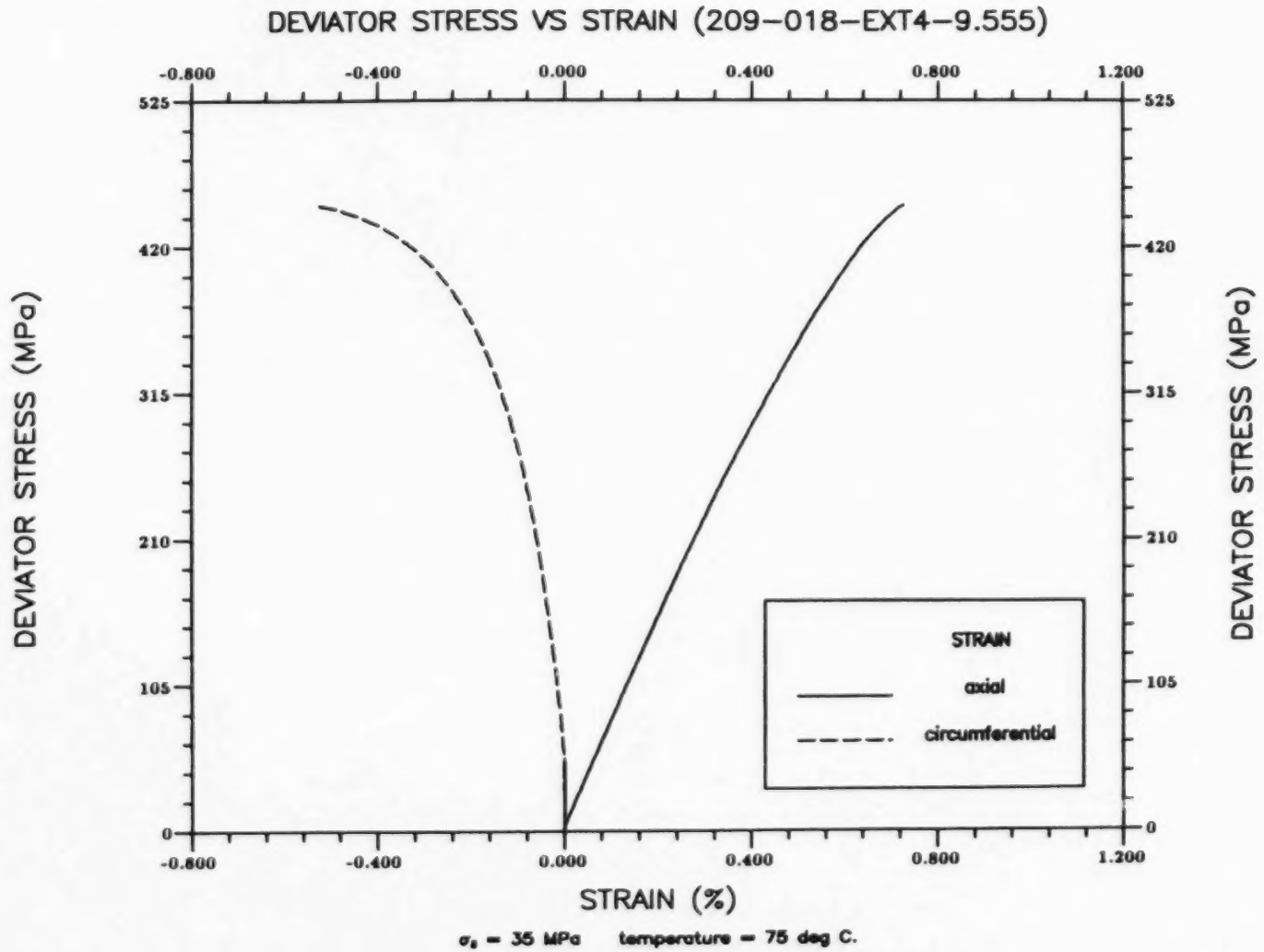

Figure A25. Stress-strain curves for Specimen 209-018-EXT4-9.555 tested at 75° C and at $\sigma_3 = 35$ MPa.

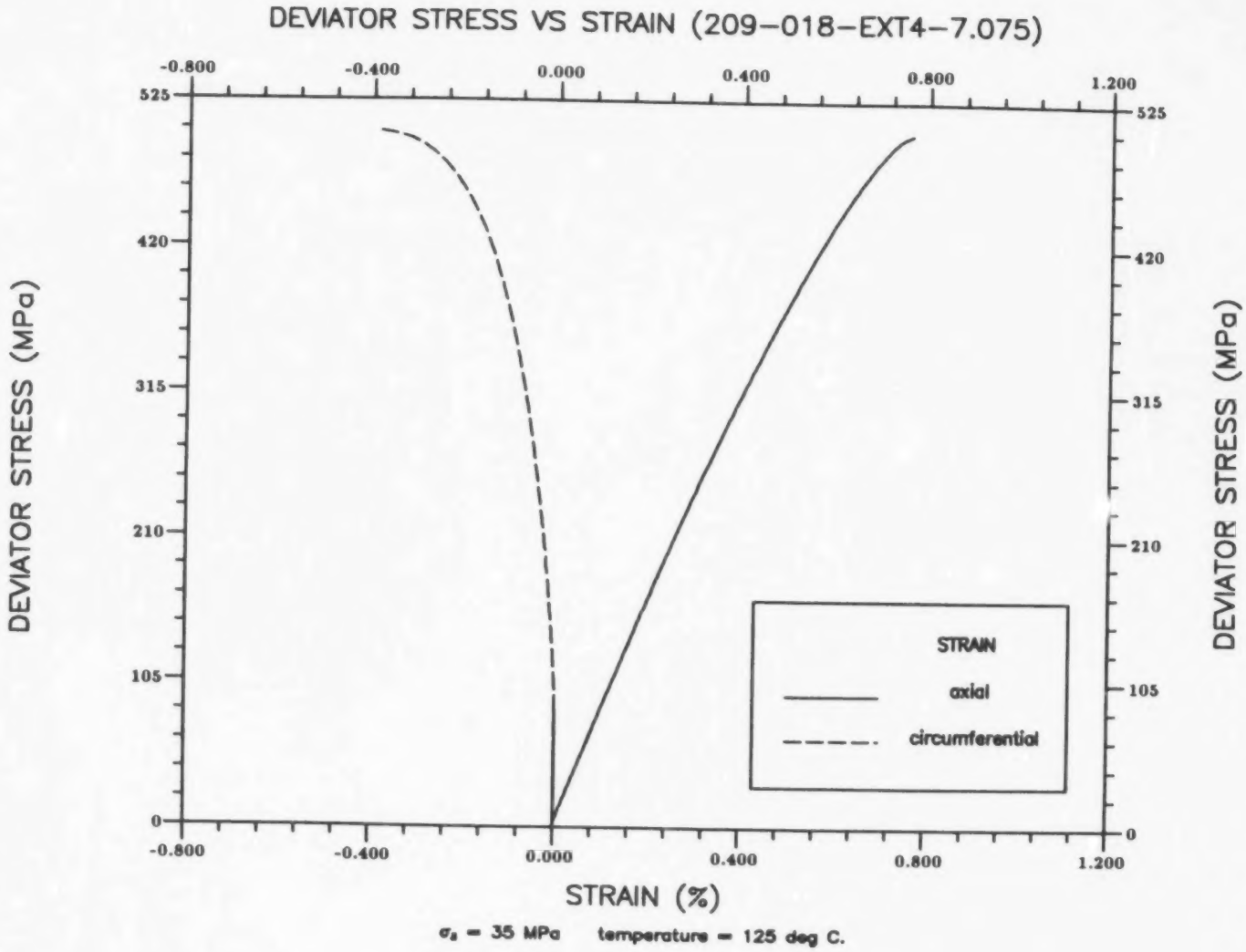

Figure A26. Stress-strain curves for Specimen 209-018-EXT4-7.075 tested at 125° C and at $\sigma_3 = 35$ MPa.

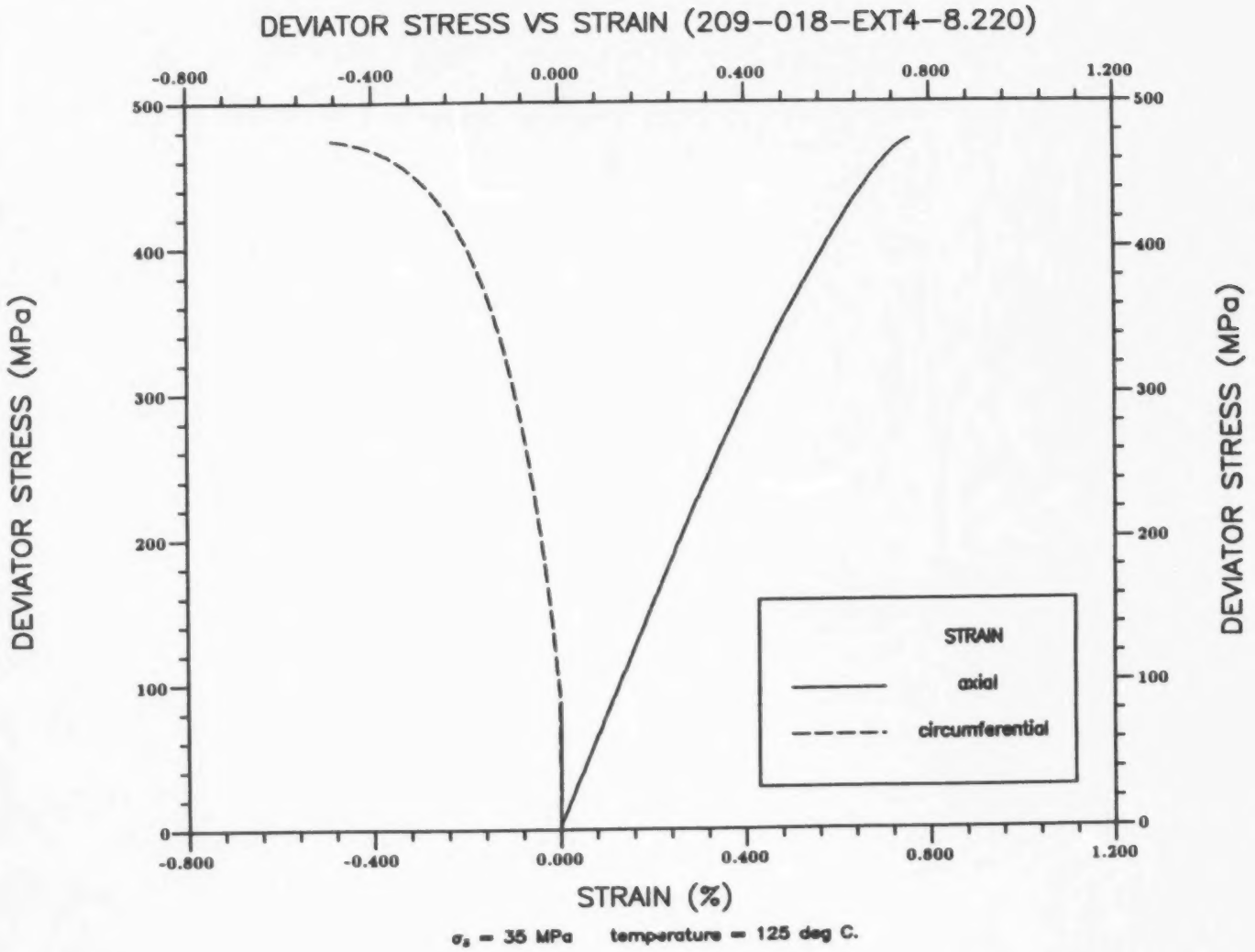

Figure A27. Stress-strain curves for Specimen 209-018-EXT4-8.220 tested at 125° C and at $\sigma_3 = 35$ MPa.

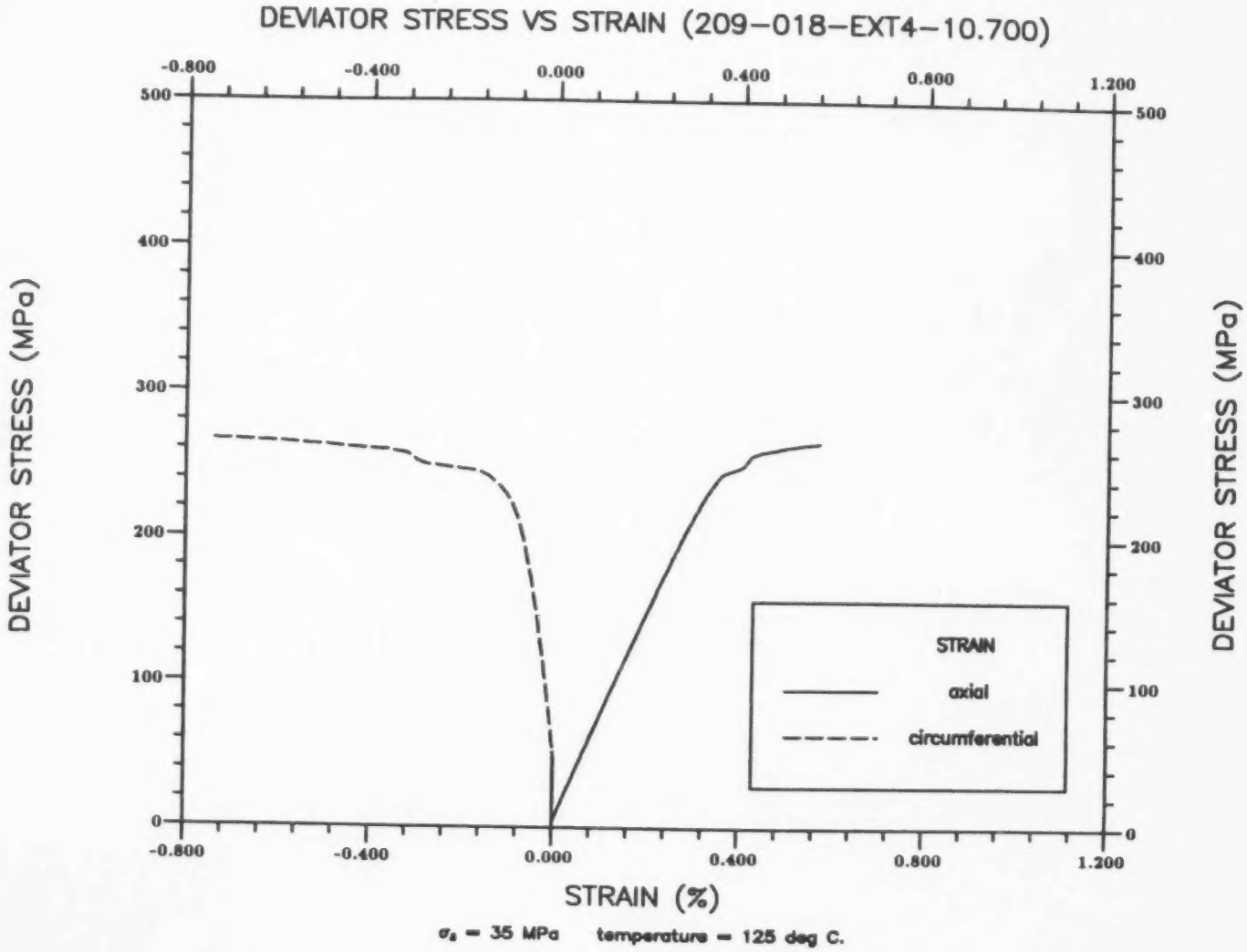

Figure A28. Stress-strain curves for Specimen 209-018-EXT4-10.700 tested at 125° C and at $\sigma_3 = 35$ MPa.